2019•2020

Faculteit Industriële ingenieurswetenschappen

master in de industriële wetenschappen: energie

Masterthesis

Tool construction for optimal transformer design

PROMOTOR :

Prof. dr. ir. Wilmar MARTINEZ

PROMOTOR :

Drs. Camilo SUAREZ

COPROMOTOR :

Prof. ir. Aniceta DEXTERS

Ruben Everaerts, Niels Martin

Scriptie ingediend tot het behalen van de graad van master in de industriële wetenschappen: energie, afstudeerrichting elektrotechniek

Gezamenlijke opleiding UHasselt en KU Leuven

2019•2020

Faculteit Industriële ingenieurswetenschappen

master in de industriële wetenschappen: energie

Masterthesis

Tool construction for optimal transformer design

PROMOTOR :

Prof. dr. ir. Wilmar MARTINEZ

PROMOTOR :

Drs. Camilo SUAREZ

COPROMOTOR :

Prof. ir. Aniceta DEXTERS

Ruben Everaerts, Niels Martin

Scriptie ingediend tot het behalen van de graad van master in de industriële wetenschappen: energie, afstudeerrichting elektrotechniek

UHASSELT

KU LEUVEN

Deze masterproef werd geschreven tijdens de COVID-19 crisis in 2020. Deze wereldwijde gezondheidscrisis heeft mogelijk een impact gehad op de opdracht, de onderzoekshandelingen en de onderzoeksresultaten.

Acknowledgements

This master's thesis marks the end of our Master's degree in engineering technology at the University of Hasselt in association with KU Leuven. It was written in context of our specialisation in Energy and Electrical Engineering. We both chose this specialisation because of the shared enthusiasm in the rapid evolution of technologies in the energy sector. The subject of the thesis seemed quite interesting as the results could prove useful to a broad audience.

Between September 2019 and June 2020, we worked hard on research, coding and writing. Near the end we did stumble on some setbacks while programming which delayed our progress for a few weeks. The unfortunate Corona Crisis also brought some minor difficulties. However, together with our promoters, we managed to fix the issues and get back on track.

This paper may interest anyone within the energy sector to gain a general understanding of efficient transformer design. A similar methodology to the one described in the paper could be applied to other electrical components which could be interesting for other studies.

We want to thank the research facility EnergyVille for permitting us to conduct this study. It has taught us a lot about power electronics, more specifically about power transformers and how to optimize them. Without our promoters at EnergyVille, Prof. Dr. ir. Wilmar Martinez and PhD. student ir. Camilo Suarez, we wouldn't have been able to finish the thesis in time. We are very grateful for their continuous support and for making time whenever we had any questions. Our third promoter, Prof. ir. Annick Dexters of the KU Leuven also deserves our gratitude. Finally, we also thank Prof. Dr. Jeroen Lievens for helping us writing the paper and organising peer sessions during the Corona lockdown.

We wish you much enjoyment in reading this master's thesis and we hope you will learn something from it.

Ruben Everaerts & Niels Martin

Contents

ACKNOWLEDGEMENTS **3**

LIST OF TABLES **7**

LIST OF FIGURES **9**

GLOSSARY **11**

ABSTRACT **13**

ABSTRACT IN NEDERLANDS **15**

1 INTRODUCTION **17**

1.1 BACKGROUND 17
1.2 PROBLEM DEFINITION 18
1.3 GOALS 18
1.4 METHOD 18

2 STUDY ON TRANSFORMER DESIGN **19**

2.1 INTRODUCTION 19
2.2 MAGNETIC CHARACTERISTICS OF MATERIALS 19
2.2.1 Theory of magnetic aspects of materials *19*
2.2.2 Classes of magnetic materials *21*
2.3 TRANSFORMER MATERIALS 22
2.3.1 Winding materials *22*
2.3.2 Core material *22*
2.4 TRANSFOMER LOSSES 23
2.4.1 Core losses *23*
2.4.2 Copper losses *24*
2.5 MODELING 25
2.5.1 First design methodology *25*
2.5.2 Second design methodology *27*

3 TRANSFORMER DESIGN **33**

3.1 PARAMETERS 34
3.2 REQUIREMENTS 34
3.3 MATERIAL PROPERTIES 35
3.4 THERMALLY LIMITED TRANSFORMER DESIGN 36
3.4.1 Heat dissipation *36*
3.4.2 Maximum allowed losses *36*
3.4.3 Peak induction *36*
3.4.4 Number of turns *38*
3.4.5 Distribution of total allowed copper losses *39*
3.4.6 Determine wire diameter *39*
3.4.7 Actual copper losses *40*
3.4.8 Check copper filling factor *41*
3.4.9 Check the core size *41*
3.4.10 Efficiency *42*
3.5 NON-THERMALLY LIMITED TRANSFORMER DESIGN 42
3.5.1 Determining core dimensions *42*
3.5.2 Determining core/copper ratio *43*
3.5.3 Number of turns, wire diameter and efficiency *45*

4 RESULTS **47**

4.1 VALIDATION 47
4.2 COMPARING RESULTS FOR DIFFERENT MATERIALS 51
4.2.1 Powder cores *51*
4.2.2 Ferrite cores *54*

4.3 EVALUATING DESIGNS WITH DIFFERENT FREQUENCY 56
4.4 EVALUATING DIFFERENT DESIGNS 59
5 CONCLUSION 61
6 FUTURE WORK 63
BIBLIOGRAPHY 65
APPENDIX A: EXCEL-FILES 69
APPENDIX B: SIMULATION PARAMETERS 77

List of tables

TABLE 1: E-CORE DIMENSIONS FOR E100/60/28 47
TABLE 2: MATLAB MODEL CONDITIONS 50
TABLE 3: DESIGN PARAMETERS OF THREE TRANSFORMERS BASED ON 50
TABLE 4: DESIGN PARAMETERS FOR THERMALLY LIMITED MODEL 50
TABLE 5: DESIGN PARAMETERS FOR NON-THERMALLY LIMITED MODEL 50
TABLE 6: MAXIMUM EFFICIENCY AND RANGE OF POWER DENSITY FOR MICROMETALS8, POWDERED IRON 18, 26 AND 52, MAGNETICS60 AND KOOL MU 75, 90, 125 52
TABLE 7: MAXIMUM EFFICIENCY AND RANGE OF POWER DENSITY FOR MOLYPERMALLOY 60, 125, 200, 300 AND 550 53
TABLE 8: MAXIMUM EFFICIENCY AND POWER DENSITY FOR MOLYPERMALLY60 FOR 25KHZ TO 200KHZ 56
TABLE 9: MAXIMUM EFFICIENCY AND POWER DENSITY FOR FERRITE F FOR 25 KHZ TO 200 KHZ 58
TABLE 10: DESIGN COMPARISON FOR MOST OPTIMAL DESIGNS 60

TABLE A1: CORE MATERIALS AND MAGNETIC PROPERTIES 69
TABLE A2: CORE DIMENSIONS FOR THERMALLY LIMITED MODEL 71
TABLE A 3: LITZ WIRE DIAMETERS AND NUMBER OF STRANDS 72

TABLE B 1: SIMULATION BODIES 77

List of figures

FIGURE 1: DUAL-ACTIVE BRIDGE CONVERTER 17
FIGURE 2: PERMEABILITY VARIOUS WITH B AND H 20
FIGURE 3: HYSTERESIS LOOP 20
FIGURE 4: CROSS SECTION OF A 5-LAYER BOBBIN 24
FIGURE 5: A) LITZ WIRE WITH STRANDS B) SOLID ROUND WIRE 26
FIGURE 6: DESIGN FLOWCHART OF MAGNETIC COMPONENT 28
FIGURE 7: FLOWCHART OF THE GENERAL STRUCTURE 33
FIGURE 8: DIMENSIONS OF E-CORE 35
FIGURE 9: RATE OF CHANGE OF FLUX DENSITY DEPENDENT ON VOLTAGE WAVEFORM 37
FIGURE 10: EFFECTIVE AREA S OF A VATAGE WAVEFORM 39
FIGURE 11: FRONT VIEW, SIDE VIEW AND TOP VIEW OF E-CORE 42
FIGURE 12: CAD MODEL OF TRANSFORMER CORE AND WINDINGS 48
FIGURE 13: MESH OF THE 3D TRANSFORMER MODEL 48
FIGURE 14: 3D FLUX REPRESENTATION IN THE CORE 49
FIGURE 15: FLUX REPRESENTATION IN THE CORE: A) CROSS SECTION OF SIDE VIEW, B) FRONT VIEW . 49
FIGURE 16: EFFICIENCY-POWER DENSITY GRAPH FOR MICROMETALS 8 51
FIGURE 17: EFFICIENCY-POWER DENSITY GRAPH FOR MOLYPERMALLOY 60 53
FIGURE 18: EFFICIENCY-POWER DENSITY GRAPH FOR HIGH FLUX 160 54
FIGURE 19: EFFICIENCY-POWER DENSITY GRAPH FOR MAG-FERRITE F 54
FIGURE 20: EFFICIENCY-POWER DENSITY GRAPH FOR PHILIPS FERRITE 3C81 55
FIGURE 21: EFFICIENCY-POWER DENSITY GRAPH FOR 3C81 (0-80°C) 55
FIGURE 22: EFFICIENCY-POWER DENSITY GRAPH FOR FAIR-RITE 77 56
FIGURE 23: EFFICIENCY-POWER DENSITY GRAPH FOR MOLYPERMALLOY60 FOR A) 25KHZ, B) 75 KHZ, C) 100 KHZ AND D) 200 KHZ 57
FIGURE 24: EFFICIENCY-POWER DENSITY GRAPH FOR MAG-FERRITE F FOR A) 25KHZ, B) 75 KHZ, C) 100 KHZ AND D) 200 KHZ 58
FIGURE 25: EFFICIENCY-POWER DENSITY GRAPH FOR EVERY MATERIAL FOR 100 KHZ AND 200 KHZ 59

Glossary

Acronyms

AC	Alternating current
DAB	Dual-active bridge
EMF	Electromotive force
HFT	High-frequency transformer
MEA	More electric aircraft

Symbols

α [Alpha]	Steinmetz's frequency exponent	–
α_i	distribution factor	–
β [Beta]	Steinmetz's induction exponent	–
γ [Gamma]	Steinmetz's exponent	–
ΔT	Temperature rise	[°C]
η	efficiency	–
μ [Mu]	permeability	[H/m] or [N/A^2]
ρ [Rho]	resistivity	[Ωm]
Φ [Phi]	magnetic flux	[Wb]
φ [phi]	phase shifting angle	[rad]
Ψ [Psi]	flux linkage	[V s]
ω [Omega]	angular frequency	[rad/s]
A	area	[m^2]
a_{ch}	largest dimension of the component	[m]
A_e	effective core area	[m^2]
B	magnetic flux density or magnetic induction	[T]
d	Primary referred output voltage	–
d_i	diameter	[m]
f	switching frequency	[Hz]
H	magnetic field	[A/m]
I_{RMS}	RMS current	[A]
k_{cu}	copper filling factor	–
k_e	Eddy current constant	–
k_h	Steinmetz hysteresis constant	–
L	inductance	[H]
L_{Ti}	mean length per turn	[m]
l_w	conductor length	[m]
N	secondary to primary turns ratio	–
n	primary to secondary turns ratio	–
n_c	number of cores	–
N_i	number of turns	–
P	power	[W]
p_i	number of strands	–
R	resistance	[Ω]
R_t	reluctance	[AT/Wb] or [1/H]
S	apparent power	[VA]
V	voltage	[V]
w_a	core window area	[m^2]
w_h	core window height	[m]

Abstract

As the demand for high-power DC applications rises, the Belgian research facility EnergyVille, located in Genk, is focussing its research onto highly efficient and lightweight DC/DC converters. Designing DC components has become increasingly difficult due to the lack of space for said electrical components and the inevitable shortage of copper and iron. This thesis has designed an algorithm that can calculate thousands transformer designs for given conditions. This programme can be used as a tool to design the most suitable transformer for a certain application.

The algorithm is made in Matlab and is validated in the simulation tool Elmer. Concretely, the algorithm calculates and compares transformer designs of different dimensions and materials so the optimal design can be chosen. This is done via two approaches, one determines the efficiency based on a maximum temperature, the other assumes external cooling, meaning lower temperature requirements, allowing more designs to be evaluated.

The results successfully show for each material the relationship between the power density, efficiency and dimensions. Secondly, the simulation ensures that the results are valid. The algorithm can evaluate designs for any kind of magnetic material, making it suitable for a broad range of applications. It serves as a basis for anyone who wants to design a transformer using any software, while no extended knowledge about transformers is needed. To conclude, the tool proves to be a good, fast and reliable way to design transformers.

Abstract in Nederlands

Door de stijgende vraag naar DC-toepassingen met grote vermogens is er binnen het onderzoekscentrum EnergyVille te Genk een grote focus naar zeer efficiënte en lichte DC/DC-omzetters. Het ontwerpen van DC-componenten wordt steeds moeilijker door het gebrek aan ruimte in bepaalde toepassingen en het dalend aanbod aan koper en ijzer. Deze thesis heeft een algoritme ontworpen dat duizenden transformatorontwerpen berekent voor bepaalde condities. Dit algoritme kan worden gebruikt als hulpmiddel om de meest geschikte transformator voor een bepaalde toepassing te ontwerpen.

Het algoritme is gemaakt in Matlab en wordt gevalideerd in de simulatietool Elmer. Concreet berekent en vergelijkt het algoritme transformatorontwerpen van verschillende afmetingen en materialen zodat het optimale ontwerp kan worden gekozen. Dit gebeurt via twee benaderingen. De ene bepaalt het rendement op basis van een maximale temperatuur, de andere gaat uit van externe koeling, waardoor er mindere temperatuur beperkingen zijn en meer ontwerpen kunnen worden geëvalueerd.

De resultaten tonen voor elk materiaal de relatie tussen de vermogensdichtheid, het rendement en de afmetingen. Daarnaast kan het ook ontwerpen voor elk soort magnetisch materiaal evalueren, waardoor het geschikt is voor een breed scala aan toepassingen. Het dient als een basis voor iedereen die een transformator wil ontwerpen, terwijl er geen uitgebreide kennis over transformatoren nodig is. Tot slot blijkt de tool een snelle en betrouwbare manier te zijn om transformatoren te ontwerpen.

1 Introduction

1.1 Background

In the last couple of decades, the demand for electrical systems in the industry in general has seen a tremendous growth. High efficiency rates have become more important due to the increase in environmental awareness and the tendency to lower costs. Higher efficiency means power losses are aimed to be reduced as much as possible. Moreover, there is a general tendency to decrease the volume or weight of the electrical systems while maintaining the power output.

To handle the increased electrical power in various systems, such as electric vehicles, power distribution systems are needed. The DC-power distribution system arises interest due to its volume and weight benefits over the AC distribution system. Another advantage of DC-systems is the absence of harmonics, DC offset and power frequency variations [1]. The DC-power distribution system consists of DC to DC converters capable of increasing or decreasing the input voltage at the output. These are widely used for the conversion from the DC network to DC-loads such as batteries and motor control. Optimising such distribution systems can prove important for many applications. EnergyVille is one of many institutions investigating this topic, more specifically highly efficient, lightweight DC/DC-converters for the More Electric Aircraft (MEA). The research facility EnergyVille is formed by the universities of Leuven and Hasselt, VITO and Imec and mainly focuses on research in sustainable energy solutions and intelligent energy systems.

There are two different types of magnetic DC-DC converters according to their magnetic component. This component can be an inductor or a transformer. This thesis will mainly focus on a dual-active bridge converter (DAB) which is a DC-DC converter with a transformer. Beside the transformer, the dual-active bridge converter also consists of other components which are shown on figure 1.

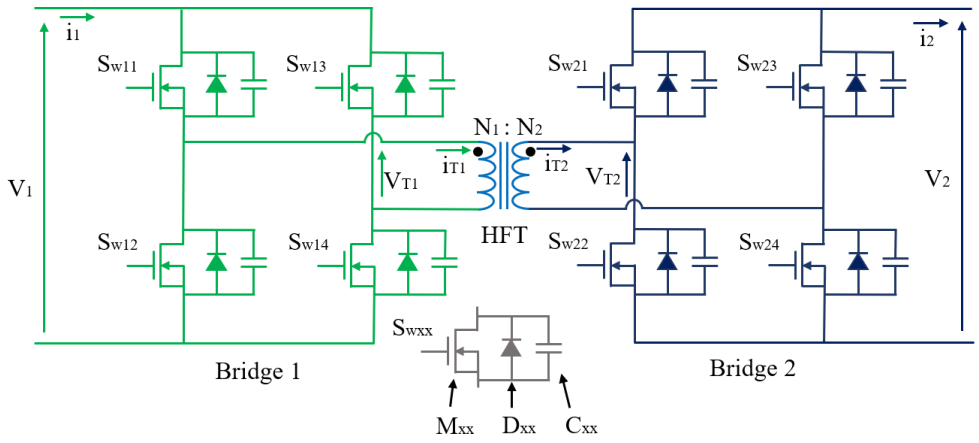

Figure 1: Dual-active bridge converter [2, p. 2311]

The converter is made up of two bridges that are connected with each other via a high-frequency transformer (HFT). This transformer provides a galvanic isolation between input and output. The bridges each consists of two voltage sources and four switches. A switch S_{wxx} comprises a Mosfet M_{xx} and parallel to the Mosfet the diode D_{xx} and the capacitor C_{xx}. By the switching action of the Mosfets a high-frequency square wave voltage is created at the primary and secondary side of the transformer. These square wave voltages are phase shifted relative to each other. If the phase-shifted angle between the two square wave voltages can be controlled, the power flow from one side of the dual-active

bridge to the other can also be regulated. This means it is possible to achieve bidirectional power transfer through the DC-DC converter.

1.2 Problem definition

Because of the increase of renewable energy sources on the grid and electrification of vehicles DC is getting more attention. The demand for high power DC-applications in these sectors is rising. To supply high enough voltages and currents, larger electrical components are required. Problems occur when these large and heavy components need to be implemented in a limited space like a car or airplane. This extra weight is in direct contradiction to reduced over-all weight and power consumption the automotive industry continuously strives towards. Trying to find a solution can prove to be quite expansive and time consuming.

A specific problem that arises attention is the charging issue for electrical vehicles. More studies are looking at ways to charge these vehicles more quickly, also known as fast charging. To supply the high-power electricity needed for this, new and better transformers are needed.

Another problem is the inevitable shortage of certain materials often used in electrical components such as copper. Right now, transformers use mostly copper. Trying to come up with an alternative design, using different materials, could take months, which increases costs.

1.3 Goals

The goal of the study at EnergyVille is to create a model for the DAB that can be used as a tool to find the optimal dimensions for the DAB in a certain situation. This thesis will mainly focus on the design optimization of the transformer of the DAB to reach the optimal efficiency for a small volume. As the volume decreases, more energy losses will occur due to temperature constraints. In other words, increasing the power density will lower the efficiency. The correlation between the power density and efficiency will eventually be simulated using Matlab. This model will then look for the optimal size of the DAB. A second condition is that the DAB should still be able to support the same amount of power as it gets smaller.

In an ongoing study at EnergyVille different materials are studied and tested with the goal to minimalize the use of copper. Using these materials will result in different core losses and thus a different efficiency. The results of these test will be used as parameters for the model. This way the optimal dimensions can be compared for the different materials.

1.4 Method

The thesis will mainly focus on the design and optimization of a transformer in Matlab. The first step will be to study theoretical literature about transformers. The transformer is used in a dual-active bridge, so the working and technical aspects of a DAB needs to be studied as well. Secondly, we will start working on the simulation code to design the transformer. This can be done with the help of a similar code for an inductor design in a boost-converter which is written by our internal promotor.

2 Study on transformer design

2.1 Introduction

To get a better understanding on how a transformer works and how to find the optimal efficiency for a small volume, many studies that have already been carried out on this subject will have to be examined. This literature study consists of four topics which are mainly important for the optimization and design of a transformer. These four topics are:

- magnetic characteristics of materials,
- materials of transformer,
- losses,
- modelling.

A transformer consists of a core surrounded by copper windings. The type of material used for the core affects a lot of parameters in the design of the transformer because every material has its own magnetic characteristics and specific material properties. That is why it is important to study the literature on different materials used as a core in transformers and its magnetic properties. The different power losses inside the transformer must also be studied to find the optimal power efficiency for a small volume. This optimal power efficiency for a small transformer volume must be modelled so that it can be used for different core materials. Therefore, modelling is an important part in this literature study.

2.2 Magnetic characteristics of materials

2.2.1 Theory of magnetic aspects of materials

Every material has different magnetic properties. In order to understand these magnetic properties, first the general theory behind magnetic characteristics needs to be studied.

Permeability is the magnetic property of a material that says how easily the magnetic flux is built up in a material, i.e. how easily a material becomes magnetized [3]. It is determined by the ratio of the flux density B in Wb/m² to the magnetizing force H in Ampere/meter. Putting this in a formula we get:

$$\mu = B/H \tag{1}$$

Permeability of a material can also be defined as $\mu = \mu_0 * \mu_r$ where μ_0 is the permeability of free space ($\mu_0 = 4\pi \times 10^{-7}$ Henry/meter) and μ_r relative permeability of the material [4]. The relationship between B and H is not linear as shown in figure 2.

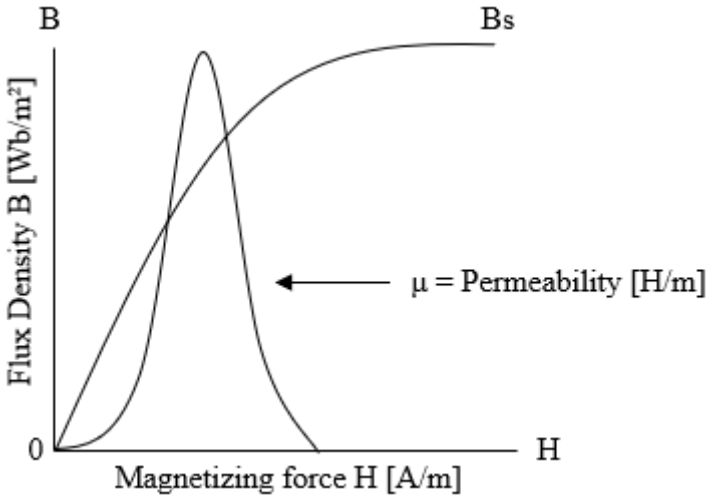

Figure 2: Permeability various with B and H [3]

The flux density B in function of the magnetizing force H is represented by the curve B_s. The other curve represents the permeability and is indicated by an arrow. The permeability can be calculated by reading B and H from the graph and filling in the formula $\mu = B/H$. Every magnetic material has a different permeability curve. Figure 2 represents a ferromagnetic material because the relative permeability is not constant. The flux density and magnetizing force for the top of the curve gives the maximum permeability. Increasing the magnetizing force after the maximum permeability lowers the permeability and the flux density becomes more and more constant. The material is saturated [5].

The hysteresis loop gives a lot of information about the magnetic properties of a material. It indicates the relationship between the magnetic field strength and the induced magnetic flux density of a material which is seen on the figure below. To understand this figure, it is important to understand how exactly magnetization of a material works. Every ferromagnetic material contains small areas in which all atoms have the same magnetic orientation. Such an area is called a magnetic domain and can be seen as a little magnet within the magnetic material. The magnetic orientations of said domains are random and differ from each other. As the material gets magnetized all these domains will orientate parallel with the external magnetic field. When this field is gone, the domains will return to their original positions [6].

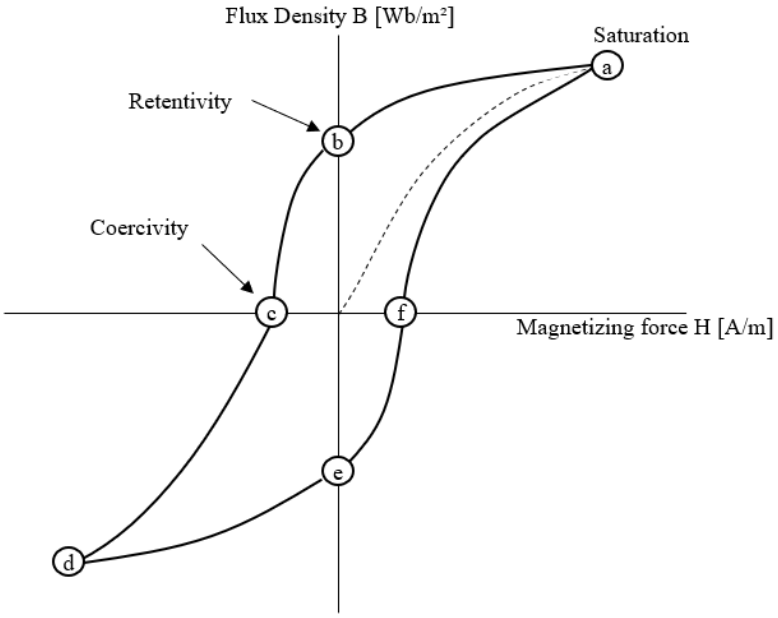

Figure 3: Hysteresis loop [5, p. 31]

A material that has never been magnetized before will follow the dotted line to point a. Increase of magnetizing force in point *a* causes a very small increase of flux density. As can be seen in Figure 3, the decrease in magnetizing force will not be proportional. Decreasing the magnetic field strength from point *a* to *b* gives higher values for the flux density than going from point zero to *a*. This can be explained by the irreversible behaviour of certain magnetic domains. The reversal of certain domains to their original position is accompanied by friction, as a result some domains remain stuck and their magnetic orientation remains unchanged. Point *b* is the remanent induction which is the magnetic induction that remains after the magnetic field strength has become zero. In order to reduce this remanent induction to zero, the magnetic material must be magnetized in the opposite direction. The coercive field strength (point *c*) is the field strength needed to cancel out the remanent induction. If the field strength continues to increase in the opposite direction, point d is reached. To reach point *a* again, everything as described above will take place but in opposite direction [7].

The remanent induction B in point b and the coercive field strength H in point c are two quality characteristics of a magnetic material. If the hysteresis loop is narrow (small B_r and H_r), it is referred to as a magnetically soft material. If the hysteresis loop is wide, it is called magnetic hard material.

Another important magnetic property is the reluctance. The reluctance is the resistance against the magnetic flux build-up in a magnetic material and is given by:

$$\mathcal{R}_t = \frac{Ampere - Turns}{\phi} \tag{2}$$

R_t is the reluctance in ampere-turns/Weber.

2.2.2 Classes of magnetic materials

The orbital and spin motions of electrons and how they will interact with other electrons will determine the magnetic aspects of a material [8]. Materials will behave differently under a magnetic field [9]. Magnetic materials can be classified into five major groups according to how they will react to the magnetic field:

- diamagnetism,
- paramagnetism,
- ferromagnetism,
- ferrimagnetism,
- antiferromagnetism.

Diamagnetism means that the atoms of the material have no magnetic moments and thus show no magnetic properties. When a magnetic field is applied the material gets magnetized in the opposite direction, meaning the material is pushed off by the external field [10].

Paramagnetic materials have unpaired electrons, therefore each atom is associated with a magnetic moment due to electron spin. Positive magnetism is caused by the fact that the dipoles start to orient themselves according to the applied magnetic field. When the magnetic field is removed, the dipoles start to reorient again. This is because the dipoles do not interact and therefore large magnetic fields are required to align all dipoles.

Due to the exchange of interaction between the dipoles, the permanent unpaired dipoles line up easily with the applied magnetic field in ferromagnetic materials. For small magnetic fields, large magnetizations can be obtained.

A ferrimagnetic material is composed of two magnetic parts A and B, separated by oxygens. The magnetic moment of A and B are not equal which result in a net magnetic moment. Ferrimagnetism has a lot of common aspects as ferromagnetism but has a very different magnetic ordering.

Antiferromagnetic is called when the exchange interactions between neighbouring atoms lead to antiparallel alignment of the atomic magnetic moment. An example of antiferromagnetic material is chromium.

2.3 Transformer Materials

2.3.1 Winding materials

As mentioned before, a transformer consists of a core material surrounded by windings on either side. The two most commonly used materials as windings in a transformer are copper and aluminium. In order to make a choice between these two materials, certain factors have to be taken into account such as maximum dimensions and weight.

In extreme conditions aluminium can have a creep rate up to 25 higher than copper. This results in aluminium wound transformers having a higher chance to failure than the copper ones. Another advantage of copper over aluminium is that copper is stronger, harder and more ductile than aluminium. But one of the most important aspects of copper is that it has a better conductivity than aluminium, resulting in lower heat losses. When designing a transformer, the size and weight of the material is also important. At first sight aluminium seems more interesting in this aspect due to its lower mass density. This, however, is cancelled out by the lower conductivity of aluminium. To conduct the same amount of current through an aluminium winding as through a copper winding, the cross-section of the aluminium conductor needs to be 1.6 times larger than that of the copper conductor. This results in a larger transformer volume when using aluminium. Due to the higher volume, transformers with aluminium windings will also have a higher weight. These are the main reasons why there will be chosen to use copper windings inside the transformer [11].

2.3.2 Core material

The core of the transformer must be magnetic in order to create a magnetic field and guide the flux through the core. The magnetic materials used for the core are classified into four groups:

- soft ferrites,
- powder iron cores,
- alloy cores,
- nanocrystalline cores.

Soft ferrite is a metal oxide which has a high electrical resistance. This result in lower eddy current or lower core losses. Ferrite cores are mainly used in high frequency applications. The most used soft ferrites are manganese-zinc ferrite (Mn-Zn) and Nickel-zinc ferrite (Ni-Zn).

Powder iron cores have a higher saturation for flux density than soft ferrites. Carbonyl iron, Sendust and Molypermalloy Powder (MPP) are the most used powder iron cores.

Alloy type cores have the highest saturation flux density and a low resistivity. The low resistance limits the application to a switching frequency of 30kHz but the high permeability allows to make the design more compact and efficient [12].

The most modern core types are nanocrystalline cores, which come with a range of advantages. Nanocrystalline cores have a flux density comparable to that of the powder iron cores and a high electrical resistivity (around 1.2 μΩcm [13]). Both the initial permeability μ_i and the remanent induction ratio B_r/B_s are controllable, making the material useful for a wide range of applications.

2.4 Transformer losses

A transformer does not have any rotating components, which means it does not have any mechanical losses. Yet, its efficiency is below 100 percent (95 to 98.5% according to [14]) due to heat losses. There are two main reasons for these losses which allows us to divide the losses into two main categories: core and copper losses.

2.4.1 Core losses

Core losses, also called iron losses, are dependent on the magnetic properties of the materials the core is made of. These losses are, however, constant as they are independent of the load. For this reason, the losses are also called no-load losses. There are two types of core losses which will be explained in detail.

Hysteresis loss is caused by the alternating magnetic field inside the core material. Current flowing through the primary winding of the transformer produces a magnetizing flux in the core. This flux induces in its turn a voltage in the secondary winding. The current in the primary is alternating (AC) meaning that the flux in the core is also alternating with the current. As explained before, when the core gets magnetized by the flux, these domains will all orientate parallel to the magnetic lines of the flux. When the current switches direction, the domains will get back to their original states before orientating again with the flux, but this time in the opposite direction. Changing the orientation of these domains requires some work. The energy needed for this is what is called hysteresis loss.
If a sinusoidal current is applied, the following equation can be used to calculate the work loss [15]:

$$P_{hys} = K_h V f B_{max}^{1,6} \tag{3}$$

K_h stands for the Steinmetz hysteresis constant, V for volume of the core in m^3, f is the frequency of the applied AC current and B_{max} is the maximum flux density the material can reach before it gets saturated.

A second core loss is known as the Eddy current loss. Like mentioned before, the magnetic flux produced by the primary current induces a voltage in the secondary winding. Though not all the energy from the flux goes to the secondary as it can also induce an electromagnetic force (emf) locally in the core itself or the metal casing of the transformer. The emf will result in a current circulating locally in the part of the transformer. These currents will dissipate as heat and are therefore considered losses. Eddy current loss can be calculated using a similar equation used for the hysteresis losses [15]:

$$P_e = K_e f^2 t^2 B_{max}^2 \tag{4}$$

The thickness of the core is represented by t and k_e stands for the Eddy current constant.

Equations (3) and (4) can only be used for sinusoidal signals. However, the input current of the transformer is not sinusoidal, therefor another equation is needed. To calculate both the eddy current and hysteresis losses another version of the Steinmetz equation will be used: the improved generalised Steinmetz equation [16].

$$P = \frac{1}{T}\int_0^T k_i \left|\frac{dB}{dt}\right|^a (\Delta B^{b-a})dt \tag{5}$$

This single equation allows one to calculate both the hysteresis and Eddy current losses for non-sinusoidal signals.

2.4.2 Copper losses

Both the primary and secondary windings are not made of ideal conductors, meaning there is some loss as current flows through them. This is what is called copper loss and comes in the form of heat. These losses depend on the resistance of the conductor and the current flowing through it. It can be calculated with a simple formula [14]:

$$P_{cu} = R * I^2 \tag{6}$$

This equation, however, is only valid for DC signals. For AC, the RMS value of the current I_{RMS} needs to be used instead. Unlike core losses, copper losses are not constant because the current, and thus the losses, depend on the load.

Another loss occurring in applications using multiple conductors and windings, is proximity loss. When a conductor is near another conductor, a current will be induced due to the varying magnetic field of the nearby conductor. This is called the proximity effect. In [17] an equation is given to calculate these losses:

$$P_p = b_w \sum_{i=1}^{n} l_i \frac{1}{h_i \sigma} H_i^2 [(1+\alpha_i^2) G_1(\Delta_i) - 4\alpha_i G_2(\Delta_i)] \tag{7}$$

Figure 4 shows a cross section of a bobbin with five layers of windings. The width and the height of the layers are respectively given by b_w and h_i. l_i represents the length of a turn.

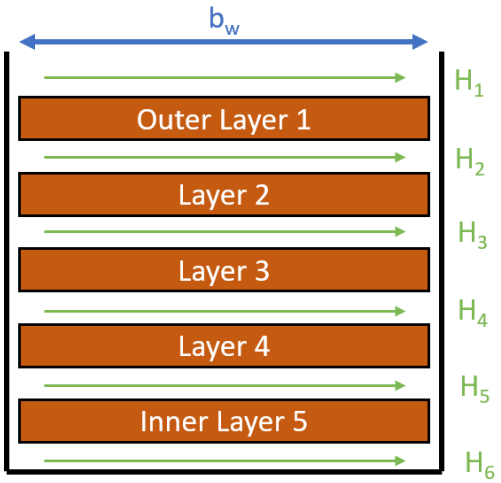

Figure 4: Cross Section of a 5-layer bobbin [15]

H_i gives the strength of the field at the edge of that layer. The ratio of the fields is given by the term α.

$$\alpha_i = \frac{H_i}{H_{i+1}} \tag{8}$$

G_1 and G_2 are both terms expressed by sines and cosiness's of Δ:

$$G_1 = \Delta \frac{\sinh(2\Delta) + \sin(2\Delta)}{\cosh(2\Delta) - \cos(2\Delta)} \tag{9}$$

$$G_2 = \Delta \frac{\sinh\Delta\ \cos\Delta + cosh\Delta\ \sin\Delta}{\cosh(2\Delta) - \cos(2\Delta)} \tag{10}$$

With Δ being the ratio of the layer's height and δ the skin depth:

$$\Delta_i = \frac{h_i}{\delta} \tag{11}$$

To understand what skin depth means, the skin effect needs to be explained. The skin effect is the tendency of alternating current to flow mostly on the outside of the inductor. The skin depth δ is the distance from the surface (skin) of the conductor to where the current density drops below 1/e (which is about 37%) of the current's value at the surface. The skin depth depends on the conductivity of the inductor material σ, the radian frequency ω and the magnetic constant $\mu_0 = 4\pi * 10^{-7}$:

$$\delta = \sqrt{\frac{2}{\omega \mu_0 \sigma}} \tag{12}$$

2.5 Modeling

In order to create a model for a transformer with the highest power density and efficiency, it is necessary to know what the important parameters are to reach this optimal point. Optimal design methodologies for a transformer will be discussed in the next section.

2.5.1 First design methodology

The first design methodology is based on [18]. In the design methodology the general parameters such as operating frequency, in- and output voltage levels, output power and transformer turn ratio are selected. Then the minimum volume meeting the efficiency and heat dissipation demands are determined by free parameters compromised of geometrical and electrical parameters. These free parameters are chosen based on the selected core material and construction. After that, one can determine all the geometrical dimensions of the transformer using the free parameters. The maximum heat dissipation of the transformer based on the free parameters is calculated and the combinations of free parameters that result in unacceptable power losses are rejected. Finally, the optimal free parameters with the highest efficiency is given.

In this design methodology of a transformer, fixed and free parameters are used. Fixed parameters are the Steinmetz constants and magnetic aspects of different magnetic materials extracted from datasheets. The transformer dimensions will be different for each material because the difference in power density

and efficiency for every magnetic material. The choice of free parameters depends mainly on the used core and windings topologies with the desired optimization goals [19]. These free parameters can be the number of magnetic core stacks, n_c , the thickness of the primary and secondary copper foils, d_{f1} and d_{f2} and the maximum allowed RMS value of the current density through a conductor, J_{max} . In high frequency applications, however, Litz wires are often used instead of standard round conductors. These kinds of conductors have a reduced influence of the skin and proximity effects. Figure 5 shows a litz wire consisting of 40 strands which are usually twisted around eachother. Litz conductors may have additional free parameters such as the number of strands, strands diameter and bundle dimensions.

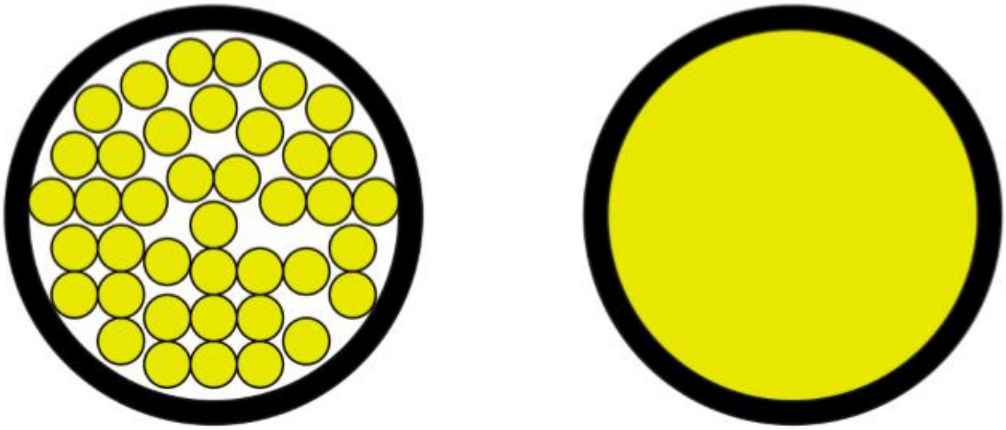

a) b)

Figure 5: a) Litz wire with strands b) solid round wire [20, p. 18]

Based on the fixed and free parameters, the transformer dimensions can be determined. One of them is the required magnetic core cross section which is defined as:

$$A_c = \frac{V_{rms1}}{k_f k_c N B_m f} \tag{13}$$

V_{rms} is the RMS value of the primary voltage, k_c the filling factor, N the number of windings, B_{max} max induction, f frequency and k_f defined as:

$$k_f = \frac{2\sqrt{2D - \frac{8R}{3}}}{D - R} \tag{14}$$

D is the duty cycle and R the rise and fall time. For rectangular waveforms is D=0.5 and R=0.

When all the geometric dimensions of the transformer are determined, the power losses can be evaluated. In this way, the efficiency and power density can be calculated. Each free parameter results in over more than thousand combinations of free parameters when implemented over a wide range of inputs. To find the optimum set, a design flowchart with all sets of free parameters will be created.

2.5.2 Second design methodology

It is important to include the eddy current losses in the design of a transformer to avoid any significant errors. The proposed thermal approach is an approach that uses a decision tree instead of a time-consuming mathematical tool. The next design methodology that will be discussed is based on [21]. This design methodology is categorized in two major cases. These are the saturated thermally limited design and non-saturated thermally limited design. The flowchart for designing a magnetic component is shown below in figure 6.

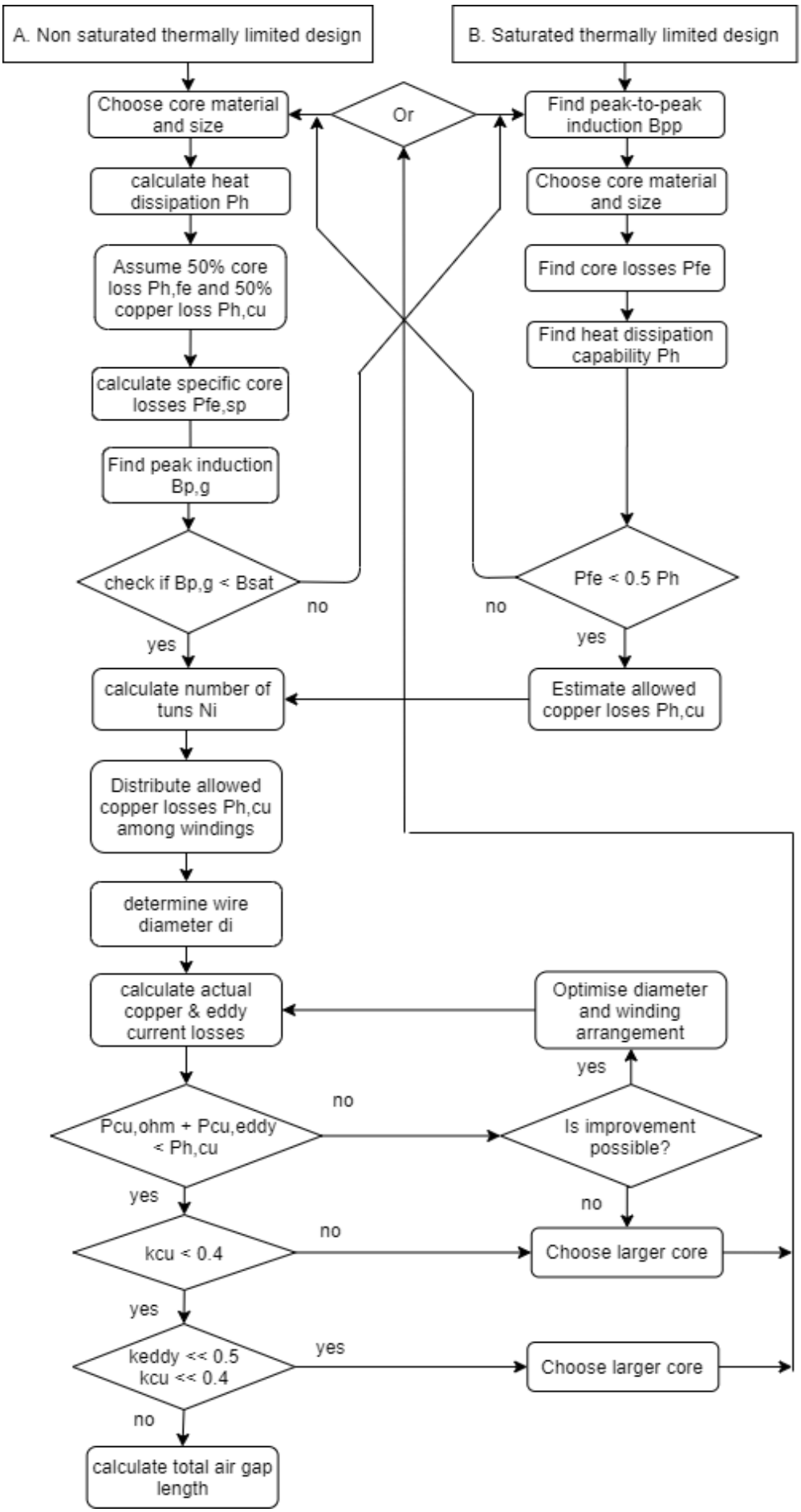

Figure 6: Design flowchart of magnetic component [21, p. 58]

Before going through this flowchart, the input parameters have to be determined. These are the RMS current of windings, peak current of windings, peak to peak flux linkage, peak flux linkage and insulation requirements. After that, one of the three design approaches is chosen. Magnetic components for high frequency AC is approached with the saturated thermally limited design, magnetic components for applications with a high DC component or low frequency applications is approached with the saturated thermally limited design and components used in audio, telephone, or radio frequency applications are approached with the signal quality limited design.

The first step of the non-saturated thermal limited design is the choose a core material and size. Using the formula below, the largest dimension of the component a_{ch} can be found at a given volt-amp rating *S*.

$$S_{tot} = \sum_{all\ windings} V_{RMS} I_{RMS} = A\, a_{ch}^{\gamma} \Rightarrow\ a_{ch} = (\frac{S_{tot}}{A})^{1/\gamma} \tag{15}$$

Where *A* is a coefficient in the range from (5-25) x 10^6 for ferrites if a_{ch} is in metres. a_{ch} is used as a scaling parameter. γ is an exponent that depends on the material, size of the core and induction B. Usually the coefficient varies from $2.8 < \gamma < 3.2$.

Secondly, the total heat dissipation capability P_h will be calculated with:

$$P_h = k_A ab \tag{16}$$

Where k_A is a coefficient, typically 2500 W/m² for the two largest dimensions *a* and *b* (in meters) of the component.

Note that equation (16) is only a rough estimation of the total heat dissipation capability. If the full surface of the component is used, it would require a lot of detailed calculations which are not relevant. The scaling parameter a_{ch} calculated in the previous step, can be used to fill in *a* and *b* in equation (16) because it represents the largest dimension of the component.

The third step is to find the optimal copper loss/core loss ratio. It can be simplified that when the copper losses P_{cu} are equal to the core losses P_{fe} , maximum efficiency is achieved. This is only true when the eddy current losses are low and the magnetic material is not saturated. With this assumption, the copper and core losses at maximum efficiency can be determined.

$$P_{h,cu} = P_{h,fe} = \frac{P_h}{2} \tag{17}$$

Where $P_{h,cu}$ are the total allowed copper losses and $P_{h,fe}$ the total allowed core losses. P_h represents the total allowed losses calculated in equation (16).

In the next two steps, first the specific core losses $P_{fe,sp}$ can be calculated with equation (18).

$$P_{fe,sp} = \frac{P_{fe}}{V_c\, s_m\, k_{ff}} \tag{18}$$

Where V_c is the volume of the core, s_m the specific mass of the magnetic material and k_{ff} the filling factor.

After that the peak induction $B_{p,g}$ for the specific core losses $P_{fe,sp}$ can be determined with the datasheets of the magnetic material that is used. If the peak induction is multiplied by two, the peak-to-peak induction B_{pp} can be obtained.

$$B_{pp} = 2\, B_{p,g} \tag{19}$$

The peak induction B_p has to be lower than the induction for saturation B_{sat}. This can be checked with the calculated $B_{p,g}$ in step five.

In step seven, the number of winding turns N_i is calculated. For symmetrical cases where B_{pp} is two times $B_{p,g}$, the number of turns at the primary side or secondary side, depending on where the total peak-to-peak flux ψ_{pp} is determined, can be calculated with:

$$N_i = \frac{\psi_{pp}}{2} \frac{1}{A_e\, B_{p,g}} \tag{20}$$

Where ψ_{pp} is the peak-to-peak magnetic flux of all winding turns ($\psi_{pp} = N\, \phi_{pp}$) and A_e the effective cross sectional area.

Now that the number of winding turns is known, the distributed allowed copper losses among the windings can be known with a coefficient α in step eight.

$$\alpha_i = \frac{N_i\, I_{rms,i}}{\sum_{i=1}^{n} N_i\, I_{rms,i}} \tag{21}$$

$$P_{h,cu,i} = \alpha_i\, P_{h,cu} \tag{22}$$

Where $I_{rms,i}$ is the root mean square current of winding i, $P_{h,cu}$ the total allowed copper losses and $P_{h,cu,i}$ the allowed copper losses of winding *i*.

After that in step nine, the wire diameter d_i can be determined with the calculated allowed copper losses for every winding. Considering that $P_{h,cu,i} = P_{h,ohm,i}$ because the eddy current losses are neglected in the wires and the only losses are the ohmic losses $P_{h,ohm,i}$.

$$d_i \geq \frac{2}{\sqrt{\pi}}\, I_{rms,i} \sqrt{\frac{\rho_c l_{Ti} N_i}{P_{cu,i}}} \tag{23}$$

Where ρ_c is the resistivity of the used material for the wires (in this case copper) and l_{Ti} the mean-length-per-turn of winding *i*.

When the diameter d_i is calculated, a practical wire diameter $d_{p,i}$ can be selected from the datasheets. This practical wire diameter $d_{p,i}$ must be higher than the calculated diameter d_i to allow some eddy current losses and at the same time not exceeding the allowed copper losses. Note that when using a Litz

type wire, equation (23) should be converted to $d^2_{p,i}\ p_i > d^2_i$ where p_i is the number of strands in the Litz wire.

In step ten, the actual copper losses P_{cu} are calculated. These actual copper losses are divided into two main losses. These are the actual ohmic losses and the eddy current losses. First, the actual ohmic losses $P_{cu,ohm}$ can be found with the formula:

$$P_{cu,ohm} = \sum_{i=1}^{all\ windings} \rho_c l_{Ti} N_i \left(\frac{4}{\pi\ d^2_{p,i}\ p_i}\right) I^2_{rms,i} \tag{24}$$

In case of a Litz wire, the mean-length-per-turn l_{Ti} is increased by 5%. The eddy current losses for round wires in a low frequency approximation is due to the uniform magnetic field component, which can be found with:

$$P_{cu,eddy} = \frac{l_w\ \frac{\pi\ d_p^4}{4}\ N^2}{48\ \rho_c} \left(\frac{2\pi\ f_{ap}\ I_{ac}\ \mu_0}{\omega}\right)^2 k_f \tag{25}$$

Where l_w is the conductor length of winding i ($l_w = N\ p\ l_T$) f_{ap} the apparent frequency for a symmetrical triangular current waveform $f_{ap} = 1.10\ f$ and for high frequency symmetrical triangular current waveform $f_{ap} = 1.025\ f$, I_{ac} the alternating current, μ_0 the permeability of vacuum, ω the minimum winding width of a coil former and k_f field factor (for transformers $k_f = 1$).

At high frequencies, due to eddy currents flow through the conductors, they will generate fields that influence the fields in the conductor itself and in the other nearby conductors. This will lead to a reduction coefficient F_T in equation (25). At low frequencies, this will lead to a reduction coefficient F_A in equation (25) because of the eddy losses caused by the local fields around the wire and not only by the traverse fields. Now that the actual ohmic losses and eddy current losses are calculated for all windings, the total copper losses can be determined by the sum of these two calculated losses.

The total copper losses must be lower than the thermally allowed copper dissipation, if not continue to step twelve, if so go to step thirteen.

$$P_{cu} \leq P_{h,cu} \tag{26}$$

In step twelve, the eddy current losses calculated in step eleven are investigated. These losses may be too high and can be reduced by increasing the diameter of the wire as far as it is tolerated by creepage distance. This might be a design solution in a single layer winding but for a two or more layers winding, it is useful to use p_i wires in parallel. This will decrease the eddy current losses because the diameter of the wires will be diminished with a factor $\sqrt{p_i}$.

Step thirteen will decide if the core window area W_a is large enough to fit all windings.

$$\sum_{i=1}^{n} p_i N_i \frac{\pi\ d^2_{i,p}}{4} \leq k_{cu} W_a \tag{27}$$

Where the filling factor k_{cu} = 0.4 for round conductors and k_{cu} = 0.4 for Litz wire. If the core window area is not large enough, a larger core will be selected or a material with lower losses or higher saturation level.

When the dimensions of the core window area are known, it must be checked if the chosen core in step one is not too high. The chosen core size is not too high when:

$$k_{eddy} = \frac{P_{cu,eddy}}{P_{cu,ohm}} = \frac{I_{ac}^2 \, k_c}{I_{dc}^2 + I_{ac}^2} \ll 0.5 \tag{28}$$

$$k_{cu} \ll 0.4 \tag{29}$$

If the core size is too high, a smaller core size alongside higher wire diameter are to be chosen.

In the last step of the non-saturated thermal limited model, the total air gap length has to be calculated. Air gaps are mostly used in inductors to avoid saturation. An air gap in transformers is only used when the transformer is subjected to a magneto-motive force. Therefore, an air gap will not be used.

3 Transformer design

Each transformer is designed using two different approaches: the thermally limited and the non-thermally limited designs. In the former a maximum temperature will be considered, while the latter considers external cooling, meaning there is no temperature limitation, allowing for a broader range of dimensions to be evaluated. The non-thermally limited design could thus potentially lead to designs with a higher efficiency.

Both approaches follow the flowchart (figure 7), which is based on [18]. Certain calculations will happen differently in the two approaches. In the next paragraphs (3.1 to 3.3) the parameters used will be explained. Paragraph 3.4 explains every step of the flowchart for the thermally limited model. The non-thermally limited model will be explained in 3.5.

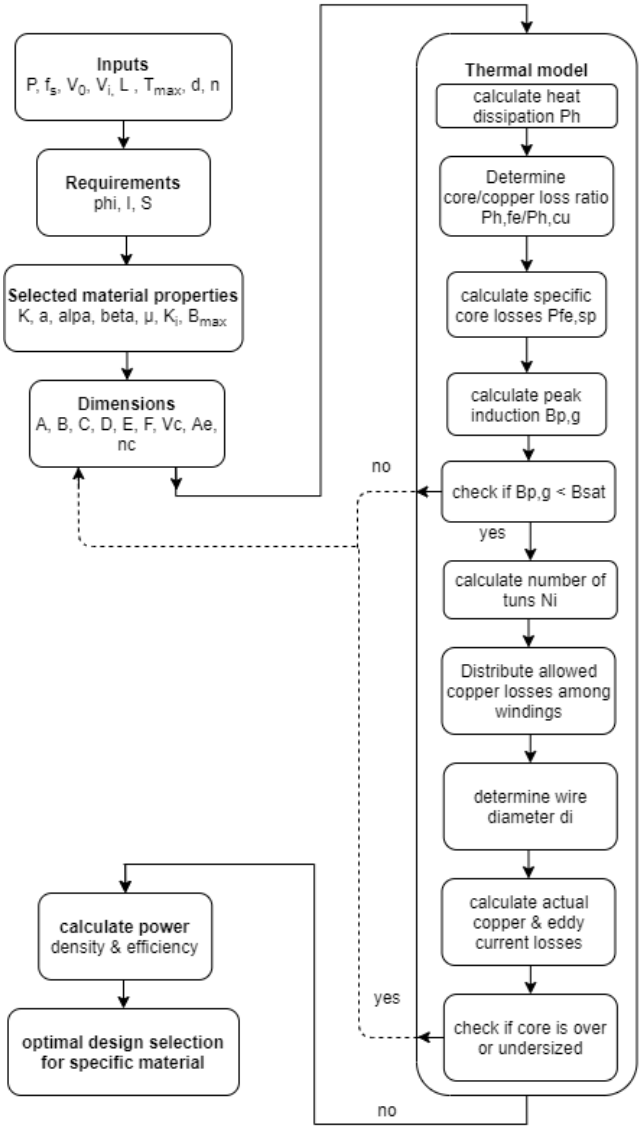

Figure 7: Flowchart of the general structure

3.1 Parameters

Before any parameter can be calculated, certain known values need to be defined. The values of the active power P, switching frequency f_s, input and output voltages V_i and V_o, leakage inductance L and the maximum temperature T_{max} need to be inserted by the user as they are unique for every application. Next the primary referred output voltage d and turns ratio n are directly derived from these inputs.

3.2 Requirements

The first step has already been discussed in 3.1 so no further explanation is needed. In step two certain quantities need to be calculated, namely the shifting angle φ, the current I_{RMS} and the apparent power S. To calculate the phase-shift angle, an equation calculating the transferred power in a DAB [22] is used:

$$P = \frac{nV_1V_2\varphi(\pi - |\varphi|)}{2\pi^2 fL} \tag{30}$$

The primary-referred output voltage to the input voltage ratio is:

$$d = \frac{V_2}{NV_1} \tag{31}$$

Note that N is the secondary to primary turn ratio whereas n from equation (30) is the primary to secondary turn ratio. Equation (31) can be converted to V_2 and replace this value in equation (30). After some rearranging we get:

$$P = \frac{V_1^2 d\varphi(1 - \frac{\varphi}{\pi})}{\omega L} \tag{32}$$

Equation (32) can now be solved to find φ.
Secondly the RMS value of the current is calculated using the following formula:

$$I_{RMS} = \frac{V_1}{\omega L}\sqrt{\frac{1}{3\pi}(\frac{\pi^3 d^2}{4} - 2d\varphi^3 + 3\pi d\varphi^2 - \frac{\pi^3 d}{2} + \pi^{\frac{3}{4}})} \tag{33}$$

Due to the voltage being a square wave, the AC current will not be perfectly sinusoidal. When the RMS value of the current is known, the total apparent power can be calculated:

$$S = 2\,V_2 d\frac{I_{RMS}}{N} \tag{34}$$

The reason why the apparent power is calculated is because it allows some kind of pre-selection of the appropriate dimensions. A minimum value for the largest dimension of a design is defined as a_{ch} :

$$a_{ch} = (\frac{S}{A_{fe}})^{\frac{1}{\gamma}} \tag{35}$$

where A_{fe} is a coefficient. For low-frequency design (20-30 kHz) low values for A, between 5-20 x 10^6, and for high-frequency design (100-500 kHz) high values of A, between 20-25 x 10^6 (if a_{ch} is in metres), are applicable. γ is equal to $3.5 - \frac{1}{\beta}$ with β a Steinmetz coefficient of the chosen material which can be found by curve fitting the material's B-H hysteresis curve or may be available from the manufacturer. It can be noticed that the coefficient γ is dependent on the core material.

A material and its properties are selected from an excel file. This file is available in appendix A. Only E-cores will be used because the literature study showed that they were mainly used in transformers with a high efficiency. The largest dimension of the chosen core can now be compared with a_{ch}. If the largest dimension of the chosen core is lower than a_{ch}, then these dimensions of this core are not evaluated and other core dimensions are chosen. It is possible that under certain conditions very few designs are evaluated. In this case a_{ch} can be divided by a factor. Now all designs with higher dimensions than $\frac{a_{ch}}{x}$ are chosen. The higher the value of x, the more dimensions are evaluated, but the longer the program takes.

3.3 Material properties

After the requirements are defined the iteration process begins. For every material, every set of dimensions will go through the next steps. First a material and its properties, which are available in appendix A, are selected after which the first set of dimensions are used for the following steps. The size of the transformer is defined by letters A to F, the meaning of which can be seen on figure 8.

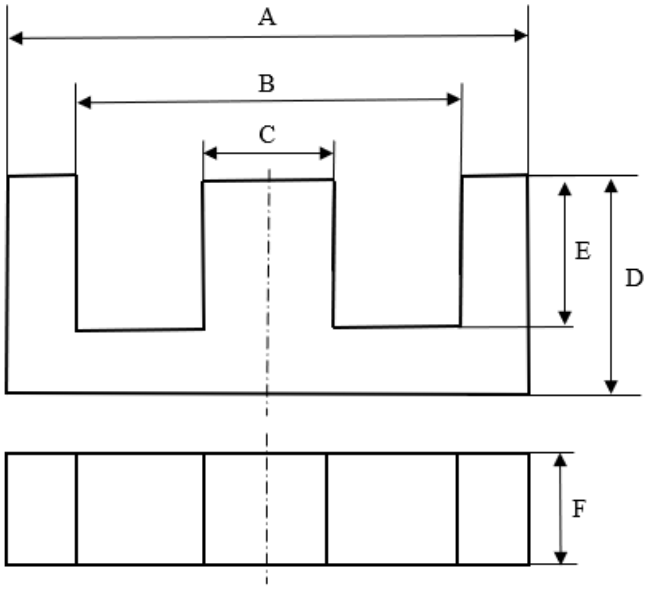

Figure 8: Dimensions of E-core [23]

These dimensions, the effective length, area and volume can be found in the datasheet of the core. These can also be calculated which will be discussed in 3.5 non thermally limited design.

3.4 Thermally limited transformer design

A template for the thermally limited design was created based on [21] which will be used as a base for both designs. In the following, each step of figure 6 will be explained in more detail for the thermally limited approach. This will give a clear picture of the content of the code.

3.4.1 Heat dissipation

The heat dissipation capability of the chosen material and dimensions is calculated in the first step of the thermally limited design. In [24] two approaches are suggested called the level 0 and level 1 thermal design. Level 0 is mathematically easier but is gives less precise results whereas level 1 requires a full calculation of the surface area. Since it is relatively easy to calculate the core's surface area the level 1 thermal design is chosen. The level 1 equation for the heat dissipation in mW is:

$$P_h = (\Delta T)^{1.1} A \tag{36}$$

ΔT is the expected temperature rise in degrees Celsius and A the total surface area in cm^2.

Formula (36) also makes it clear why this method is thermally limited. A maximum temperature rise must first be given in order to determine the heat dissipation and specific losses in the next steps. The value of ΔT is chosen by the user, though it is important to note that it must be within a certain range. The higher the temperature rise the more it can influence the flux. At a certain value, which depends on the chosen material, the core gets saturated. This is, of course, undesirable. A good estimation for a maximum temperature is 100 °C as most magnetic materials are still able to operate perfectly around this value. The temperature rise is the difference between the maximum and the ambient temperature. As an example, a temperature rise of 60 °C means that the transformer can operate up to 40 °C of the ambient temperature.

3.4.2 Maximum allowed losses

In the simplified case, maximum efficiency is close to the point where the copper losses are equal to the core losses. So the maximum allowed copper and core losses are defined as 50% of the total heat dissipation calculated in the previous step. The maximum core losses are then divided by the core's volume, giving the specific core losses.

$$P_{fe,sp,v} = \frac{P_{fe}}{V_c n_c} \tag{37}$$

V_c is the volume of one core and n_c is the amount of cores stacked next to each other.

3.4.3 Peak induction

In contrary to [21] the peak induction can be calculated using the Steinmetz's equation:

$$P_{fe,sp,v} = k\, f^{\alpha}\, B_{p,g}^{\beta} \tag{38}$$

k, α and β are magnetic properties, unique for every material and are made available in appendix A. However, this original Steinmetz equation cannot be used because it only applies to sinusoidal excitations [25]. The transformer in the DAB is fed with non-sinusoidal waveforms. Therefore, the improved generalized Steinmetz equation, also called iGSE, is used:

$$P_v = \frac{1}{T}\int_0^T k_i \left|\frac{dB}{dt}\right|^{\alpha} (\Delta B)^{\beta-\alpha} dt \tag{39}$$

Where

$$k_i = \frac{k}{(2\pi)^{\alpha-1}\int_0^{2\pi}|\cos(\theta)|^{\alpha}\, 2^{\beta-\alpha} d\theta} \tag{40}$$

The rate of change of the flux density $\left|\frac{dB}{dt}\right|$ can be determined using figure 9 if a three-level excitation voltage waveform is considered.

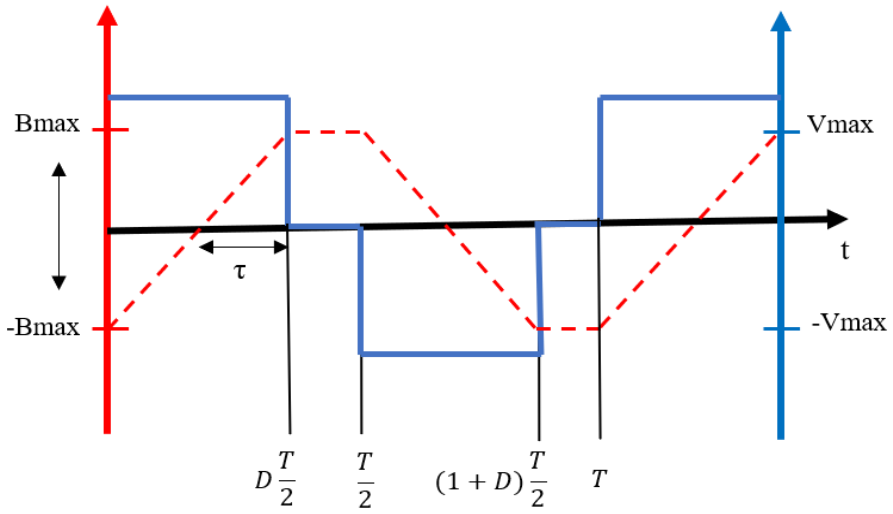

Figure 9: rate of change of flux density dependent on voltage waveform [25, p. 37]

The difference between B_{max} and $-B_{max}$ is the peak to peak flux density ΔB which can be calculated with [25]:

$$\Delta B = \frac{V_{max} DT}{N_i A_e 2} \tag{41}$$

Next, the change in flux can be determined for a certain period of time with figure 9:

$$\frac{dB}{dt} = \begin{cases} \frac{V_{DC}}{N_i A_e}, 0 \le t \le D\frac{T}{2} \\ 0, D\frac{T}{2} \le t \le \frac{T}{2} \\ \frac{-V_{DC}}{N_i A_e}, \frac{T}{2} \le t \le (1+D)\frac{T}{2} \\ 0, (1+D)\frac{T}{2} \le t \le T \end{cases} \tag{42}$$

Now the iGSE formula can be simplified by substituting equation (41) and (42) in (39). This results in:

$$P_{v,iGSE} = k_i(\Delta B)^{\beta-\alpha}\frac{1}{T}\left[\int_0^{DT/2}\left|\frac{\Delta B}{DT/2}\right|^{\alpha} dt + \int_{DT/2}^{(1+D)T/2}\left|\frac{\Delta B}{DT/2}\right|^{\alpha} dt\right] \tag{43}$$

$$P_{v,iGSE} = k_i(\Delta B)^{\beta-\alpha}\frac{1}{T}[|2\Delta B|^{\alpha}(DT)^{1-\alpha}] \tag{44}$$

Calculating the peak induction rather than getting it from a datasheet allows us to alter the frequency more easily. Every magnetic material has a specific value of inductance above which the core gets saturated. It is important for the peak induction to never exceed this value. If this is the case, larger dimensions are chosen as can be seen in the flowchart.

3.4.4 Number of turns

Since the waveforms are not sinusoidal the standard EMF-equation for transformers cannot be used. The peak to peak flux linkage is used instead:

$$\Psi_{pp} = N_i \Phi_{pp} \tag{45}$$

N_i is the number of turns in the primary or secondary and ϕ_{pp} the peak to peak magnetic flux. The latter is by definition equal to the peak to peak magnetic induction multiplied by the effective area:

$$\Phi_{pp} = B_{pp} A_e \tag{46}$$

As mentioned before the peak to peak induction B_{pp} equals two times the peak inductance $B_{p,g}$. N_i can now be calculated by substituting this information and (46) in (45):

$$N_i = \frac{\Psi_{pp}}{\Phi_{pp}} = \frac{\Psi_{pp}}{2 n_c A_e B_{p,g}} \tag{47}$$

The value of ψ_{pp} is the only unknown. By definition, this is the effective area S of the voltage over half a period as can be seen in figure 10. A simple integral is used to calculate the peak to peak flux linkage. However, since the transformer is considered a part of a DAB in this paper, the voltage can be assumed to be a square wave. In this case the integral can be simplified.

$$\Psi_{pp} = \int_{t_1}^{t_2} v(t)dt \; = \; V_2 \frac{T}{2} d \tag{48}$$

V_2*d is used because ψ_{pp} is referred to the secondary as the leakage inductace is modeled in the primary side.

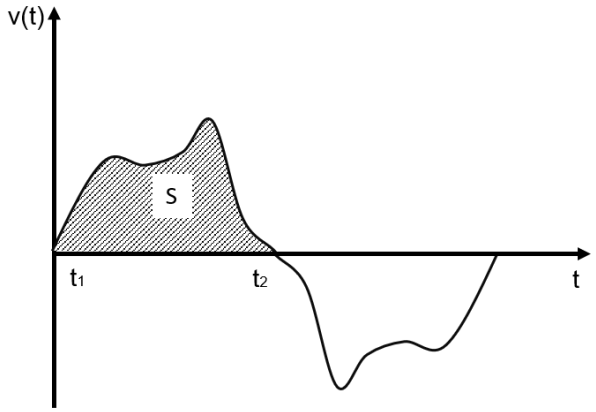

Figure 10: Effective area S of a voltage waveform [21, p. 64]

3.4.5 Distribution of total allowed copper losses

To withstand the resistance and thus the heat of the current, the wire needs to be chosen big enough. A simple solution is to take a wire with a large enough diameter and use it on both the primary and secondary side of the transformer. This, however, is expensive and impractical, as the diameter is much larger than the minimum required diameter. In order to choose the correct wire, the allowed copper losses in both the primary and secondary need to be determined. A factor $\alpha_i$is introduced to distribute the maximum allowed copper losses $P_{h,cu}$ (= P_h/2) over the primary and secondary windings.

$$\alpha_i = \frac{N_i I_{RMS,i}}{\sum_{i=1}^{n} N_i I_{RMS,i}} \tag{49}$$

N_i and $I_{RMS,i}$ are respectively the number of turns, which is calculated in the previous step, and the RMS current of winding *i*. The factor α gives the contribution of winding i to the total allowed copper losses. The allowed copper losses in winding *i* can be calculated by multiplying α_i with the allowed total losses.

$$P_{cu,i} = \alpha_i P_{h,cu} \tag{50}$$

3.4.6 Determine wire diameter

In the next step the diameter of the wire can be determined. The eddy current losses are neglected, thus the total losses equal the ohmic losses $P_{cu,ohm,i}$.

$$P_{cu,i} = P_{cu,ohm,i} = R_{0,i} I_{RMS,i}^2 \tag{51}$$

R_0 is the DC resistance of winding *i* and can be calculated using the following equation:

$$R_{0,i} = 4\rho_c \frac{L_{Ti} N_i}{\pi d_i^2} \tag{52}$$

ρ_c is the resistivity of copper, L_{Ti} the mean length per turn of the winding and d_i the diameter. After substituting (52) in (51) and solving the equation to d_i we get:

$$d_i \geq \frac{2 I_{RMS,i}}{\sqrt{\pi}} \sqrt{\frac{\rho_c L_{Ti} N_i}{P_{cu,i}}} \tag{53}$$

d_i represents the minimum required diameter to withstand the losses.

Other kinds of wires that can be used in a transformer are the litz wire or parallel wires. After calculating the minimum required diameter, the diameter of a single litz strand or single wire $d_{p,i}$ is calculated using:

$$d_{p,i}^2 p_i > d_i^2 \tag{54}$$

The number of wires in parallel or the number of strands in a Litz wire is represented by p_i and is an input. The code will search for the right type of litz wire with an individual strand diameter of at least $d_{p,i}$ and a number of strands equal to p_i, in a datasheet based on [26].

3.4.7 Actual copper losses

Now the actual copper losses of the transformer can be calculated. The ohmic copper losses are determined using the same equations as before, namely (51) and (52).

$$P_{cu,ohm} = \sum_i 4\rho_c \frac{L_{Ti} N_i}{\pi d_{p,i}^2} I_{RMS,i}^2 \tag{55}$$

In the case of this thesis i is equal to 1 or 2, representing the primary or the secondary winding. The actual copper losses can be written as the sum of the copper losses in the primary and secondary windings. In reality, a wire with a larger diameter than the one calculated in the previous step is chosen to make sure it can withstand the resistance. $d_{p,i}$ is the next available wire diameter which is higher than d_i.

Secondly the eddy current losses are calculated using the following equation [21]:

$$P_{cu,Eddy,i} = \frac{l_w N_i^2 \pi d_{p,i}^4 / 4}{48\rho_c} \left(\frac{2\pi f I_{RMS,i} \mu_0}{2 w_h} \right)^2 k_f \tag{56}$$

l_w is the conductor length of the ith winding, which is equal to mean length per turn L_{Ti} multiplied by the number of turs N_i. w_h the height of the core window and k_f is a factor which equals to 1 for transformers. One complete core comprises two E-cores, thus the total height of the core window w_h is multiplied by 2. Some designs use parallel wires or Litz wires. In these cases, a different value for the diameter d_p must be used, which is calculated using (54). Equation (54) is substituted in (55) and (56).

$$P_{cu,ohm} = \sum_i 4\rho_c \frac{L_{Ti} N_i}{\pi d_{p,i}^2 p_i} I_{RMS,i}^2 \tag{57}$$

$$P_{cu,Eddy,i} = \frac{l_w N_i^2 \pi (d_{p,i}\sqrt{p_i})^4/4}{48\rho_c} \left(\frac{2\pi f I_{RMS,i}\mu_0}{2w_h}\right)^2 k_f \tag{58}$$

The sum of the ohmic copper losses and the eddy current losses equals the total copper losses.

3.4.8 Check copper filling factor

In previous steps the diameter and amount of turns of the wires have been determined. In this step we examine whether the wires actually fit in the transformer by checking if the core window area w_a is big enough.

$$\sum_i p_i N_i \pi \frac{d_{p,i}^2}{4} \leq k_{cu} w_a \tag{59}$$

k_{cu} is the maximum copper filling factor and is equal to 0,4 for round wires and 0,2 for Litz wires. If this condition is met the code will continue, if not it will dismiss this particular design and alter the dimensions.

3.4.9 Check the core size

Finally, the code checks whether the core is not too large. The ratio of the eddy current losses (equation (58)) and the ohmic copper losses (equation (57)) is checked. If the ratio is lower than 5% the core is too high and a smaller one needs to be chosen. When the core window is barely filled (k_{cu} < 0,04) the core is also too high.

$$\frac{P_{cu,Eddy}}{P_{cu,ohm}} < 0{,}05 \tag{60}$$

$$\frac{1}{w_a} \sum_i p_i N_i \pi \frac{d_{p,i}^2}{4} < 0{,}04 \tag{61}$$

If both (60) and (61) are true, a smaller core is chosen.

After this final step, it is concluded that the chosen core dimensions are neither too large nor too small. A list of suitable core dimensions alongside its wire dimensions is composed. In order to calculate the efficiency and power density for these dimensions as accurate as possible, the losses will be recalculated using different approaches

3.4.10 Efficiency

Finally, the efficiency of the transformer design with a certain power P can be calculated:

$$\eta = \left(\frac{P - P_{tot}}{P}\right) 100\% \tag{62}$$

P is the electrical power of the transformer and is inserted as an input to the program. The sum of the total copper losses, calculated in 3.4.7, and the core losses P_{fe} gives the total losses of the design P_{tot}.

3.5 Non-thermally limited transformer design

A non-thermally limited design allows to create a transformer design with smaller or larger dimensions than the thermally limited model because the temperature is not limited. This will result in a higher power density.

3.5.1 Determining core dimensions

First, the core dimensions evaluated in the thermally limited model are divided or multiplied by a factor to get a smaller or larger design. This factor can vary from 1.1 to 1.5 depending on how many core sizes one wants to evaluate. This will also change the effective length, effective area and effective volume. Therefore, these have to be recalculated. This can be done using Figure 11.

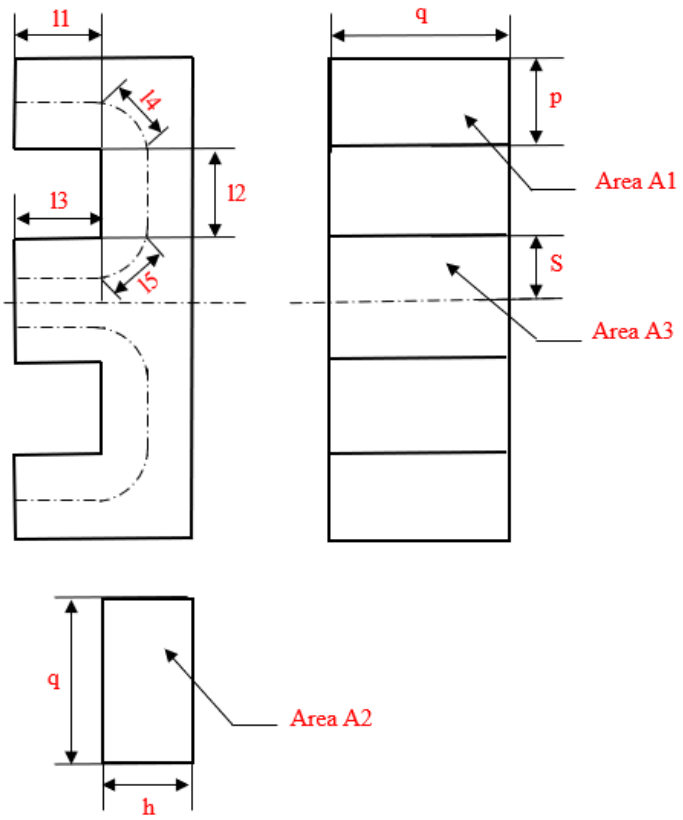

Figure 11: front view, side view and top view of E-core [27, p. 10]

In order to calculate the effective volume V_e of the E-core, the effective area A_e and effective length or also called the mean length of the flux path l_e must first be calculated. As can be seen in Figure 11, the total effective length of the core can be determined by taking the sum of l_1, l_2, l_3, l_4 and l_5 and then multiply the result with 2. Where l_4 and l_5 are equal to:

$$l_4 = \frac{\pi}{8}(p + h) \tag{63}$$

$$l_5 = \frac{\pi}{8}(s + h) \tag{64}$$

The effective areas associated with l_4 and l_5 can be determined with:

$$A_4 = \frac{A_1 + A_2}{2} \tag{65}$$

$$A_5 = \frac{A_2 + A_3}{2} \tag{66}$$

Now that every effective length and area is known, the total effective area can be determined with the following coefficients C_1 and C_2 calculated with [27]:

$$C_1 = \sum_{1}^{5} \frac{l_1}{A_1} \tag{67}$$

$$C_2 = \sum_{1}^{5} \frac{l_1}{2A_1^2} \tag{68}$$

Dividing C_1 by C_2 gives the total effective area of the core. The total effective volume of the core can also be calculated with these coefficients or by multiplying the total effective length by the total effective area.

$$V_e = l_e A_e = \frac{C_1^3}{C_2^2} \tag{69}$$

3.5.2 Determining core/copper ratio

As this model is not thermally limited, it may exceed the maximum allowed losses of $P_h/2$. Therefore, a new core/copper loss ratio must be set up that can go higher than $P_h/2$, while ensuring maximum efficiency. To recalculate this ratio, first the total losses need to be known. The total losses are determined by taking the sum of the calculated core and copper losses. A factor ε can be introduced to adjust these core and copper losses [28]. Then the total losses are:

$$P_{tot} = \frac{P_{fe}}{\varepsilon^{\beta}} + P_{cu}\varepsilon^{\gamma} \tag{70}$$

Factor ε is the relative number of turns:

$$\varepsilon = \frac{N + \Delta N}{N} = \frac{N_{new}}{N_{old}} \tag{71}$$

and γ a coefficient which value is in range of 1-3. This value depends on the constraint for example constant copper volume, constant wire section or as a result of eddy current calculation.

When the number of turns is increased by a factor ε, the induction in the core is decreased by a factor ε since the flux linkage is constant. So the induction is proportional to $\varepsilon^{-\beta}$. But on the other hand, as can be seen in equation (70), the copper losses are proportional to ε^{γ} . The ability to adjust the core and copper losses by changing the number of turns gives more freedom in designing the transformer and finding the optimal design.

The total losses P_{tot} should be minimal for $\varepsilon = 1$ for an optimal design. To get these minimal core and copper losses, the derivative of P_{tot} with respect to ε is taken.

$$\frac{d}{d\varepsilon}\left(P_{fe} + P_{cu}\right) = 0 \tag{72}$$

$$\frac{P_{fe,opt}}{P_{cu,opt}} = \frac{\gamma}{\beta}\varepsilon^{\gamma+\beta} \tag{73}$$

Substituting $\varepsilon = 1$ in equation (73) gives:

$$\frac{P_{fe,opt}}{P_{cu,opt}} = \frac{\gamma}{\beta} \tag{74}$$

Then the optimal core and copper losses for maximum efficiency are:

$$P_{cu,opt} = \frac{\gamma}{\gamma + \beta}P_{tot} \tag{75}$$

$$P_{cu,opt} = \frac{\beta}{\gamma + \beta}P_{tot} \tag{76}$$

It is assumed that there are low eddy current losses, so these losses are neglected. One can change the number of turns without changing the diameter of the wire because for most high frequency transformers the winding area is not completely filled. For this condition, a coefficient value of $\gamma = 1$ is employed. Substituting this value in equations (75) and (76) gives:

$$P_{fe,opt} = \frac{1}{1 + \beta}P_{tot} \tag{77}$$

$$P_{cu,opt} = \frac{\beta}{1 + \beta}P_{tot} \tag{78}$$

Now the specific core losses can be calculated by dividing $P_{fe,opt}$ by the effective volume and the number of cores. By filling in these specific losses in equation (39), the optimal magnetic peak to peak induction can be known. If this optimal induction is higher than the allowed saturation flux of the material, the core losses must be reduced by a factor ε until the calculated induction is lower than the saturation induction. As discussed before, this can be done by increasing the number of turns which results in lower core losses and higher copper losses.

3.5.3 Number of turns, wire diameter and efficiency

If the number of turns is not adjusted, these can be calculated equally as described in section 3.4.4 with equation (47). If the number of turns needed to change to lower the core losses, the new number of turns can be calculated with equation (71).

The minimal wire diameter can be calculated as described in section 3.4.6 . After that, the copper losses are calculated with the number of turns based on 3.4.7. Now, the total losses can be determined by taking the sum of the copper and core losses.

The efficiency of the transformer design is calculated using the same method as described in 3.4.10.

Above a temperature of 200 °C, most materials will not operate effectively. For this reason, only if the temperature rise is lower than 200 °C, the code will go back to the first step of the non-thermally limited design. The core dimensions are once again divided by a factor ranging from 1.1 to 1.5. The temperature rise can be calculated with:

$$\Delta T = \left(\frac{P_{tot}}{A}\right)^{0.833} \tag{79}$$

with P_{tot} equal to the total losses and A equal to the surface area of the core.

If the temperature rise is higher than 200 °C, the dimensions are reset to the dimensions that were evaluated in the thermally limited design. Now, instead of dividing with a factor, the dimensions are multiplied by a certain factor to evaluate higher dimensions. The same process as described above to obtain the optimal efficiency is applied. If the efficiency drops below a certain percentage the code will go back to the beginning of the thermally limited model where it starts evaluating other dimensions. This percentage is an input and its value is chosen by the user to exclude designs with a lower efficiency.

4 Results

Based on previous chapter, an algorithm was created for modelling a power transformer. This chapter will first validate the results obtained and then evaluate them.

One way to validate the obtained results is with the open source multiphysical simulation software Elmer. With this software the flux in the magnetic core can be simulated. This gives a better picture of how the transformer works and can also be compared with the flux determined in the Matlab model to validate the algorithm. Section 4.1 will go into more detail about the validation. Another way to validate the results of the Matlab model is by comparing them with other studies.

In order to evaluate the results, different materials are compared with one another. More specifically, in 4.2, the compassion between thermally limited and non-thermally limited designs for both powder and ferrite cores are made. A transformer can also work under different frequencies. The influence of increasing the frequency with different types of materials is discussed in 4.3. Finally, a brief overview on the impact of both the chosen material and frequency on the transformer design is given in 4.4.

4.1 Validation

In order to simulate the flux in the core with the simulation software Elmer, a 3D model of a transformer must first be made. This can be done with the open-source parametric 3D modeller FreeCAD. The material chosen is the powder core Molypermalloy 300. There is no specific reason why this material is used. The relative permeability μ_r equals 300 and the chosen dimensions for this specific design are shown in Table 1.

Table 1: E-core dimensions for E100/60/28 [23]

Dimensions for E100/60/28						
	Nom	**Tol +**	**Tol -**	**Max**	**Min**	**Unit**
A	100.30	2.00	2.00	102.30	98.30	mm
B	73.15	1.15	1.15	74.30	72.00	mm
C	27.50	0.50	0.50	28.00	27.00	mm
D	59.40	0.47	0.47	59.87	58.93	mm
E	46.85	0.38	0.38	47.23	46.47	mm
F	27.50	0.50	0.50	28.00	27.00	mm

The meaning of parameters A to F are visualized in Figure 8 in chapter 3.3. Based on these dimensions, the 3D model can be created which is seen on Figure 12. This CAD model consists of two E-cores stacked on top of each other, forming an EE-core, and two windings around the middle core leg.

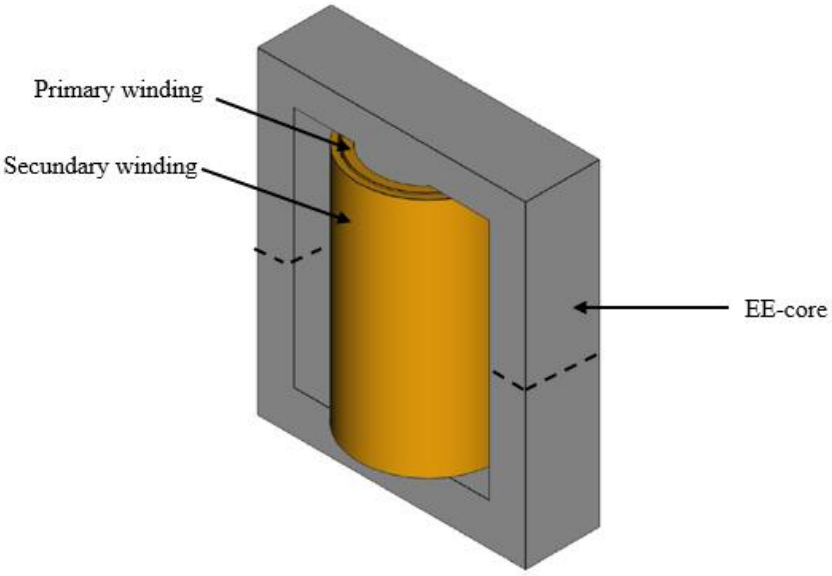

Figure 12: CAD model of transformer core and windings

This CAD model cannot be imported directly into Elmer because Elmer can only conduct simulations on meshes. Therefore, a mesh of this CAD model must be created first. A mesh is a collection of different faces, edges and vertices that define the shape of the object. The transformer mesh is made using the open-source software Salome which supports pre-processing for numerical simulation. Once the mesh is created, it can be opened in Elmer to start the simulation.

By assigning the current-density to the vertical plane (coloured red in Figure 13) of the cross-sections of both the primary and secondary windings, the flux in the core can be simulated. Figure 14 shows the result of the simulation in 3D and Figure 15 the front view and cross section of the middle leg. The settings of the Elmer simulation are given in Appendix B. These settings are mostly based on [29] and [30].

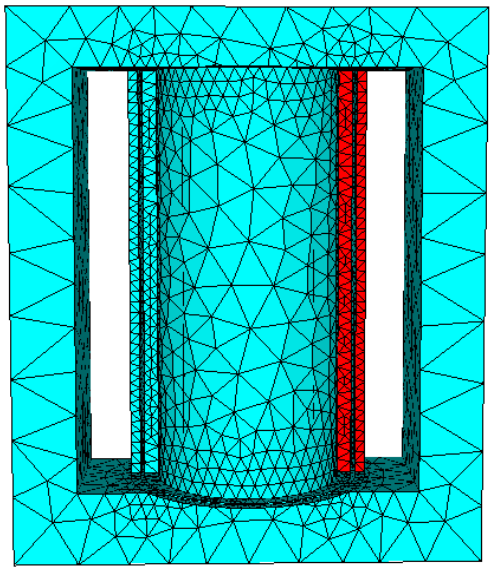

Figure 13: Mesh of the 3D transformer model

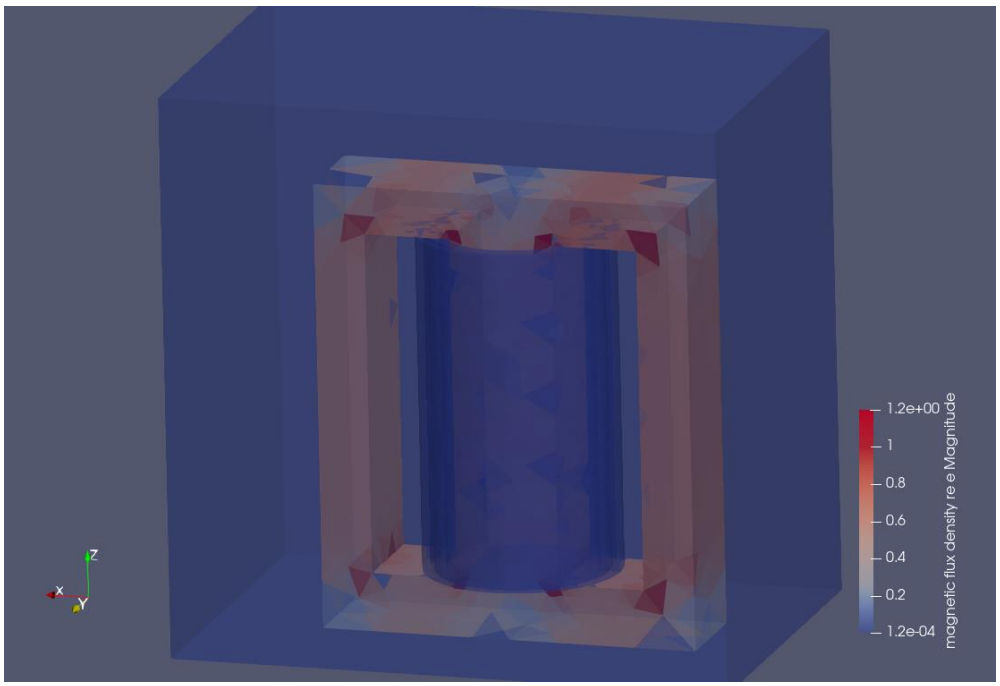

Figure 14: 3D Flux representation in the core

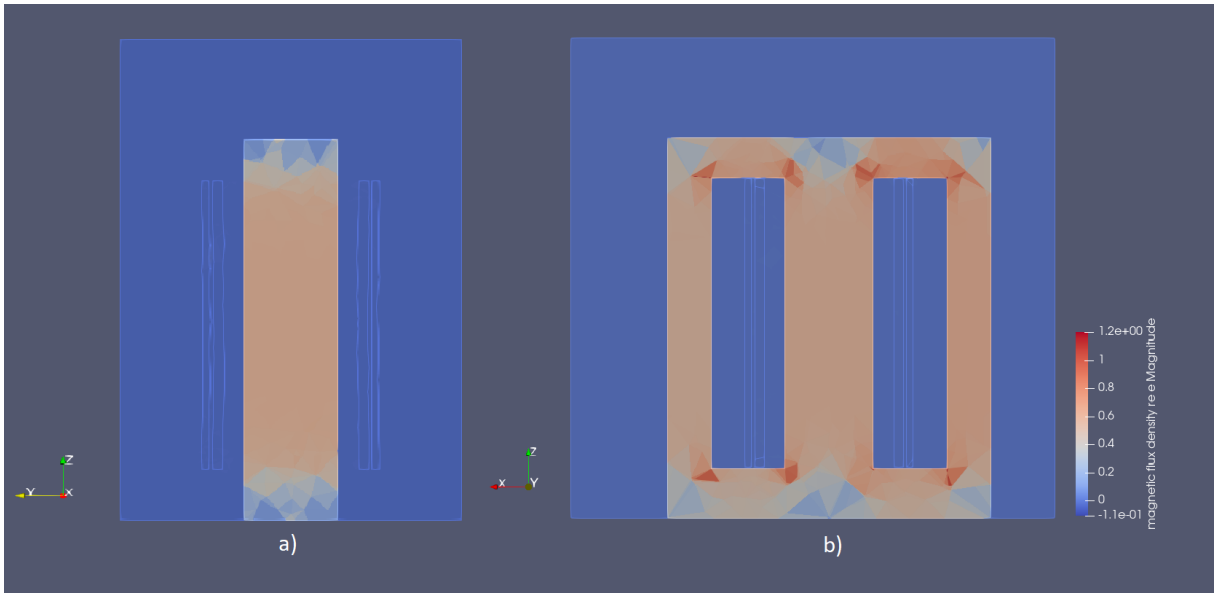

Figure 15: Flux representation in the core: a) cross section of side view, b) front view

As can be seen on Figure 14 and Figure 15, the flow of the current in the windings induces a flux in the middle of the core. The induced flux then follows a path through the two outer legs of the core. The average flux in the core legs is around 0.7 T which is lower than the saturation flux of 0.8T for Molypermalloy 300. For the non-thermally limited model the flux is equal to 0.52 T and for thermally limited it equals 0.64 T. The latter is close to the result of the simulation, which proves that the algorithm is correct. The lower flux for the non-thermally limited model can be explained by the different core/copper ratio, as explained in 3.5.2. The conditions used in the code are shown in Table 2. This simulation was done for a few other materials. The results were consistently close to the results of the Matlab code. Because of this, it can be concluded that the simulation serves as a validation for our result. However, to get an extra validation, the result is also compared with other studies.

Table 2: Matlab model conditions

Parameter	Value
Switching frequency	20 kHz
Power	10 kW
Input voltage	400 V
Output voltage	800 V
Number of strands	90
Inductance	16 µH

Table 3 contains parameters for three different transformer designs based on results from [31]. The transformers operate with V_1 = 300 V and V_2 = 100 V with a total power of 1200 W and are made of the ferrite core material N87. The three designs are compared to the results of the created thermally (Table 4) and non-thermally limited (Table 5) designs under the same operating conditions. The temperature rise for the thermally limited approach is chosen at 40°C. Also, for this comparison the eddy current losses were excluded, as these were not present in [31].

Table 3: Design parameters of three transformers based on [31]

Design		Core dimensions (mm)	Flux density B (T)	Number of turns prim/sec	Core losses (W)	Copper losses (W)
Frequency (kHz)	Core type					
25	E-core	65/32/27	0.14	32/11	5.807	5.462
50	E-core	55/28/21	0.122	36/12	3.792	3.771
100	E-core	55/28/21	0.085	26/9	3.792	3.532

Table 4: Design parameters for thermally limited model

Design		Core dimensions (mm)	Flux density B (T)	Number of turns prim/sec	Core losses (W)	Copper losses (W)
Frequency (kHz)	Core type					
25	E-core	65/32/27	0.11	69/23	5.71	4.98
50	E-core	55/28/21	0.07	75/25	3.85	3.46
100	E-core	55/28/21	0.05	60/20	3.85	3.68

Table 5: Design parameters for non-thermally limited model

Design		Core dimensions (mm)	Flux density B (T)	Number of turns prim/sec	Core losses (W)	Copper losses (W)
Frequency (kHz)	Core type					
25	E-core	65/32/27	0.09	81/27	3.46	7.21
50	E-core	55/28/21	0.06	90/30	2.33	4.15
100	E-core	55/28/21	0.04	69/23	2.33	5.28

It is noticeable that the total losses (the sum of the core and copper losses) from Table 4 and Table 5 are about equal, which indicates that both the thermally limited and non-thermally limited models calculate the losses correctly. The copper losses in Table 4 are always lower than the corresponding core losses. This is because the maximum allowed copper losses are equal to $P_h/2$, which is equal to the core losses. For the non-thermally limited model, the maximum copper losses are not limited by 50% of the total losses, therefore these losses can go higher. The results of Table 4 are not exactly the same as in Table 3, but it is close enough to give an indication of the model's accuracy. The difference in results can be

explained by the lower flux densities in this thesis's model, which is caused by the different use of Steinmetz values for K_i, α and β. These values were not known for the given materials and were thus estimated. Another reason may be that [31] employs a sinusoidal waveform for the current while this thesis focusses on a not perfectly sinusoidal waveform. The reason it is not perfectly sinusoidal is because the transformer is used in a DAB. The transistors in the DAB provide a block-shaped voltage waveform and therefore also an imperfect sinusoidal current waveform.

Nevertheless, the values obtained from both Matlab models correspond well with the design parameters presented in [31]. Based on the simulation and the tables above, it can be assumed that the both the thermally and non-thermally limited models are accurate and reliable.

4.2 Comparing results for different materials

This datasheet of the materials is based on [32] and contains a limited number of materials. Its purpose is to test the model but can be expanded in the future. In 4.2.1 and 4.2.2, the results of designs are discussed. However, the focus of this chapter is to show that the model can be used to validate designs of many different materials, rather than focussing on the results and materials themselves.

The list of materials, found in appendix A, is composed of two main types of material, namely powder iron and ferrites. Some materials give similar results, so not every single one is discussed in detail. For these comparisons only the materials and their properties are variable. Other parameters are fixed and are given in Table 2.

4.2.1 Powder cores

Figure 12 shows the efficiency and power density graph for Micrometals 8. Every dot represents one transformer design with a certain set of dimensions. The non-thermally limited designs are coloured according to the temperature rise ΔT. This term is explained in more detail in 3.4.1. The colour legend can be seen right next to the graph. In this specific example, the two darker coloured dots represent designs calculated by the thermally limited model with a temperature rise set at 60°C. All of the other designs are evaluated by the non-thermally limited model.

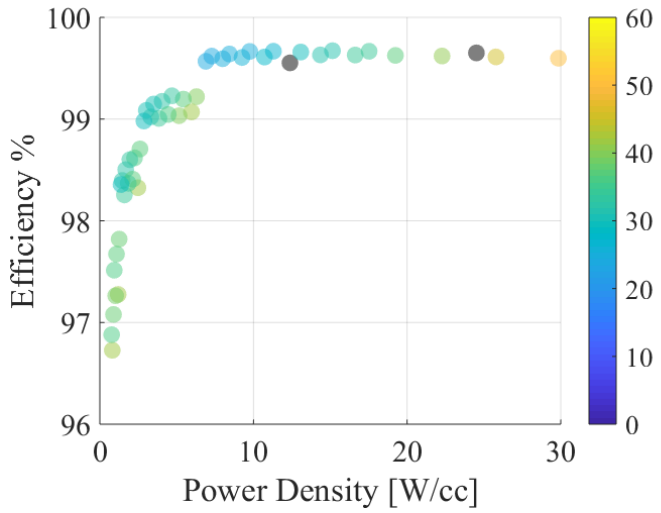

Figure 16: Efficiency-Power density graph for Micrometals 8

A lot more non thermally limited designs were evaluated than thermally limited designs, which was the exact purpose of this approach. The reason only two thermally limited designs were calculated is because the value of x (as discussed in 3.2) is set to 2. Only if the largest dimension of a design exceeds the value of $\frac{a_{ch}}{x}$ it is chosen and evaluated. If an additional cooling system is not desired (e.g. too high cost), the design choice is limited to only thermally limited designs, or to non-thermally limited designs with a low enough temperature rise. In this specific case, not a single design exceeds a temperature rise of 60°C, mainly due to the relatively low frequency.

It is noticeable that the efficiency is quite high (exceeding 99% for power densities over 3 W/cc). This is, however, not a surprise as transformers tend to have high efficiencies [33]. As the power density rises, so does the efficiency. However, after a certain power density the efficiency drops again. This can be explained by equation (47) in section 3.4.4, which shows that the number of turns increases with decreasing surface areas. At a certain point the increase in turns is higher than the decrease in length of the turns, which results in an increase in copper loss. For Micrometals 8 this tipping point is 11,3 W/cc. For power densities lower than 5 W/cc, the efficiency drops rapidly. The actual losses are derived from the maximum allowed losses, which are directly proportional with the surface are of the core. The core losses are assumed at a certain fraction of the total allowed losses and the only difference between the actual and maximum copper losses is the wire diameter. As a result, the actual losses are close to the maximum allowed losses, making the efficiency drop as the size, and thus the surface area, increase.

The graphs for all the Powdered Iron cores, Magnetics 60 and the Kool Mu materials are not shown as they are quite similar to figure 12. Instead the maximum efficiency and power density range for these materials are shown in Table 6.

Table 6: Maximum efficiency and range of power density for Micrometals8, Powdered iron 18, 26 and 52, Magnetics60 and Kool Mu 75, 90, 125

Material	**Maximum efficiency (%)**	**Maximum power density (W/cc)**
Micrometals 8	99,67	30
Powdered Iron 18	99,64	25
Powdered Iron 26	99,49	20
Powdered Iron 52	99,59	25
Magnetics 60	99,78	40
Kool Mu 75, 90 and 125	99,78	40

All three variants of the Kool Mu material behave similarly and are thus put in one row.

At first glance, prove the most interesting as these have the highest efficiencies and power densities. However, the most appropriate design depends on the applications. It is up to the user to determine which design is most interesting.

The next five materials are variants of Molypermalloy: Molypermalloy 60, 125, 200, 300 and 550. Once again, the number after the word represents the value of the permeability. Unlike the Kool Mu materials, the permeability is not the only difference. Other material properties like α, β and k_i also differ, resulting in unique graphs. Figure 17 shows the graph for Molypermalloy 60.

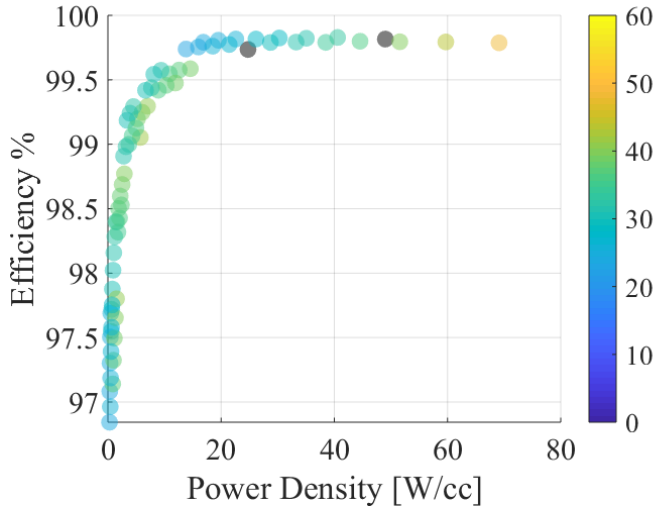

Figure 17: Efficiency-Power density graph for Molypermalloy 60

All five materials result in quite similar designs, hence only one figure is shown. Table 7 shows the differences for the five materials.

Table 7: Maximum efficiency and range of power density for Molypermalloy 60, 125, 200, 300 and 550

Material	**Maximum efficiency (%)**	**Maximum power density (W/cc)**
Molypermalloy 60	99,83	70
Molypermalloy 125	99,80	50
Molypermalloy 200	99,74	35
Molypermalloy 300	99,74	35
Molypermalloy 550	99,67	30

The higher the permeability, the lower the maximum power density making Molypermalloy 60 and 125 more interesting for applications where space is an issue. The efficiency drops as well, albeit with a very small amount (0,13% between 60 and 550).

Finally, the graph of High Flux 160 is given in Figure 18. Once again, the results for all the High Flux materials (14, 26, 60, 125 and 160) are quite similar.

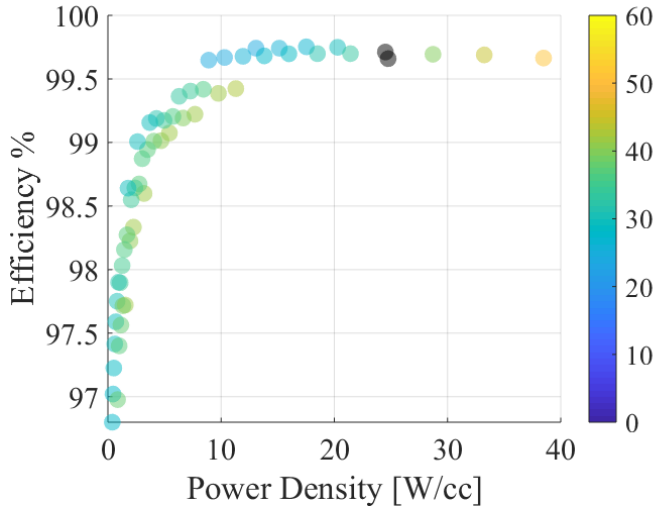

Figure 18: Efficiency-Power density graph for High Flux 160

4.2.2 Ferrite cores

The rest of the list comprises ferrite materials. The result of one such material, Mag-Ferrite F can be seen in Figure 19. At first glance the graph looks much like the figures from the powder iron materials. However, more designs exceed the efficiency value of 99.5% than in the case of powder iron cores. The maximum efficiency even reaches a value of 99,86%. Additionally, the designs can reach much higher power densities. However, when a lower power density is required, Mag-Ferrite *F* may not be ideal as the efficiency drops rapidly below a power density of about 30.

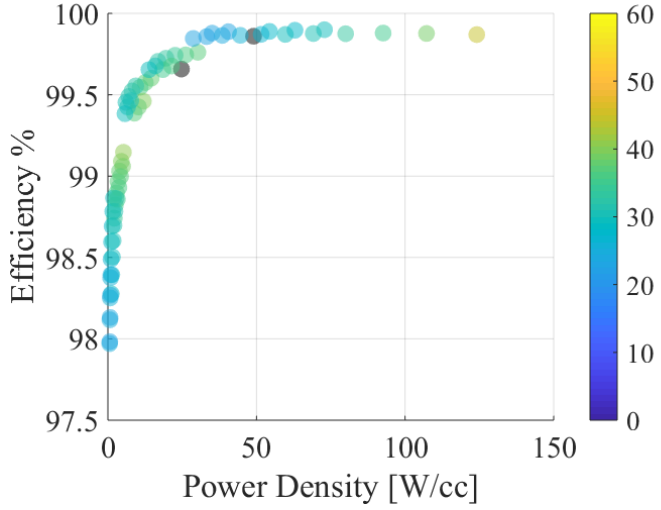

Figure 19: Efficiency-Power density graph for Mag-Ferrite F

The graph for Philips Ferrite 3C81 (Figure 20) shares many similarities with Mag-Ferrite F. However, the maximum power density is a bit lower and the maximum efficiency is reached around a power density of 40 W/cc. For Mag-Ferrite F this maximum lies around 60 W/cc. This material could be more interesting when lower power densities are required, though the user may also choose a powder iron core instead.

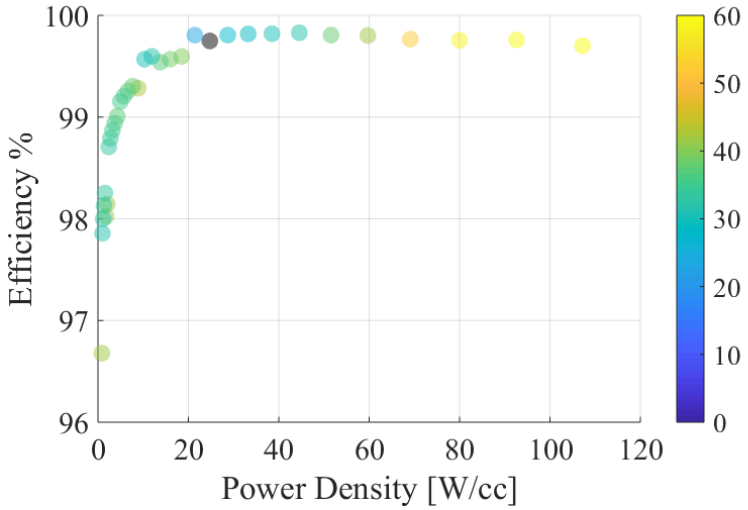

Figure 20: Efficiency-Power density graph for Philips Ferrite 3C81

Some yellow dots are present in Figure 20, which may indicate a temperature rise higher than 60°C. It is possible to adjust the temperature scale for the figures. As can be seen in Figure 21, the temperature scale as been changed to a maximum of 80°C. The three designs with the highest power density could indeed reach a temperature rise of over 60°C. These designs are therefore unsuitable for applications where no cooling is applied.

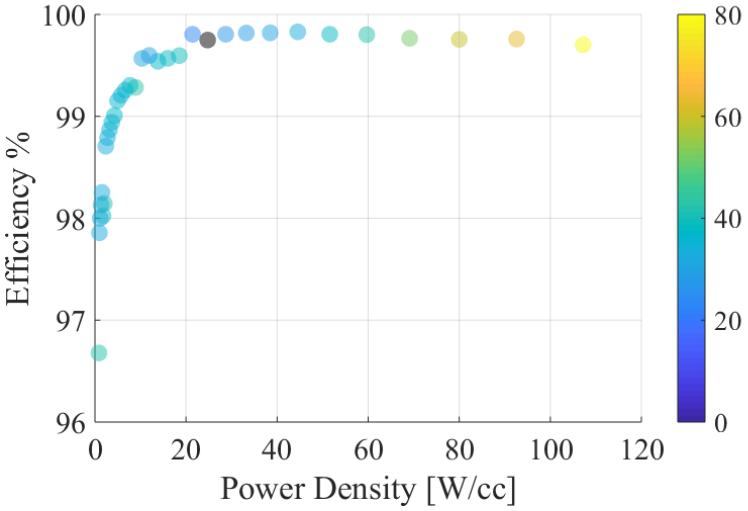

Figure 21: Efficiency-Power density graph for 3C81 (0-80°C)

Finally, the results for the ferrite Fair-Rite 77 is displayed in Figure 22. The graph is quite similar to those for powder iron materials. The efficiency starts dropping quicker and the maximum power density is lower than the two previous mentioned ferrite cores. Note that the temperature scale has increased to a maximum of 90°C, indicating that this material tends to heat more easily.

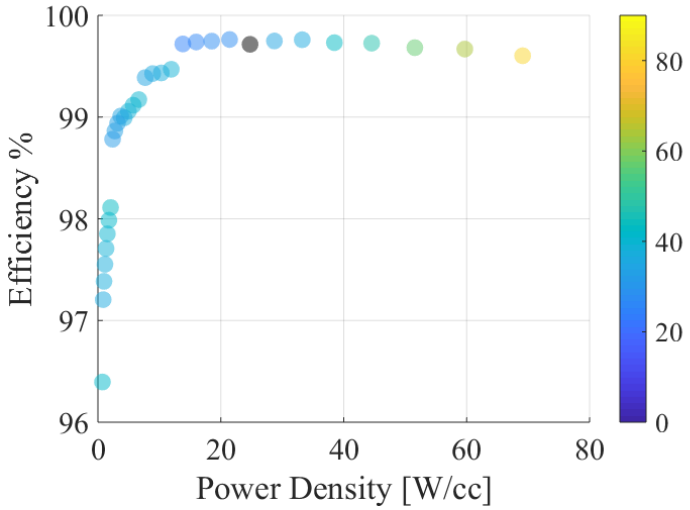

Figure 22: Efficiency-Power density graph for Fair-Rite 77

It can be concluded that ferrite cores prove to be more interesting due to their higher efficiencies and power densities. When space or weight is an issue, these materials are more useful as transformer cores than powder iron. Though, as proven by the material Fair-Rite 77, not all ferrites share this conclusion. It should be noted that this conclusion is only valid for this specific set up of 10 kW and 50 kHz.

4.3 Evaluating designs with different frequency

In the previous section different materials were compared with each other, in this section the influence of different operating frequencies on the efficiency and power density is examined.

In this first example, the frequency is incrementally increased by 25 kHz in four steps for a 10 kW transformer with material Molypermalloy 60, as can be seen in the Table 8. Also, 200 kHz is added to the table to show the influence of a much higher frequency. Figure 23 visualizes the designs for 25, 75, 100 and 200 kHz. The figure for Molypermalloy 60 with a frequency of 50 kHz was already given in section 4.2.1 (Figure 17).

Table 8: Maximum efficiency and power density for Molypermally60 for 25kHz to 200kHz

Frequency (kHz)	Max efficiency (%)	Power density (W/cc)
25	99,65	15-20
50	99,83	40
75	99,86	52
100	99,86	54
200	99,76	21

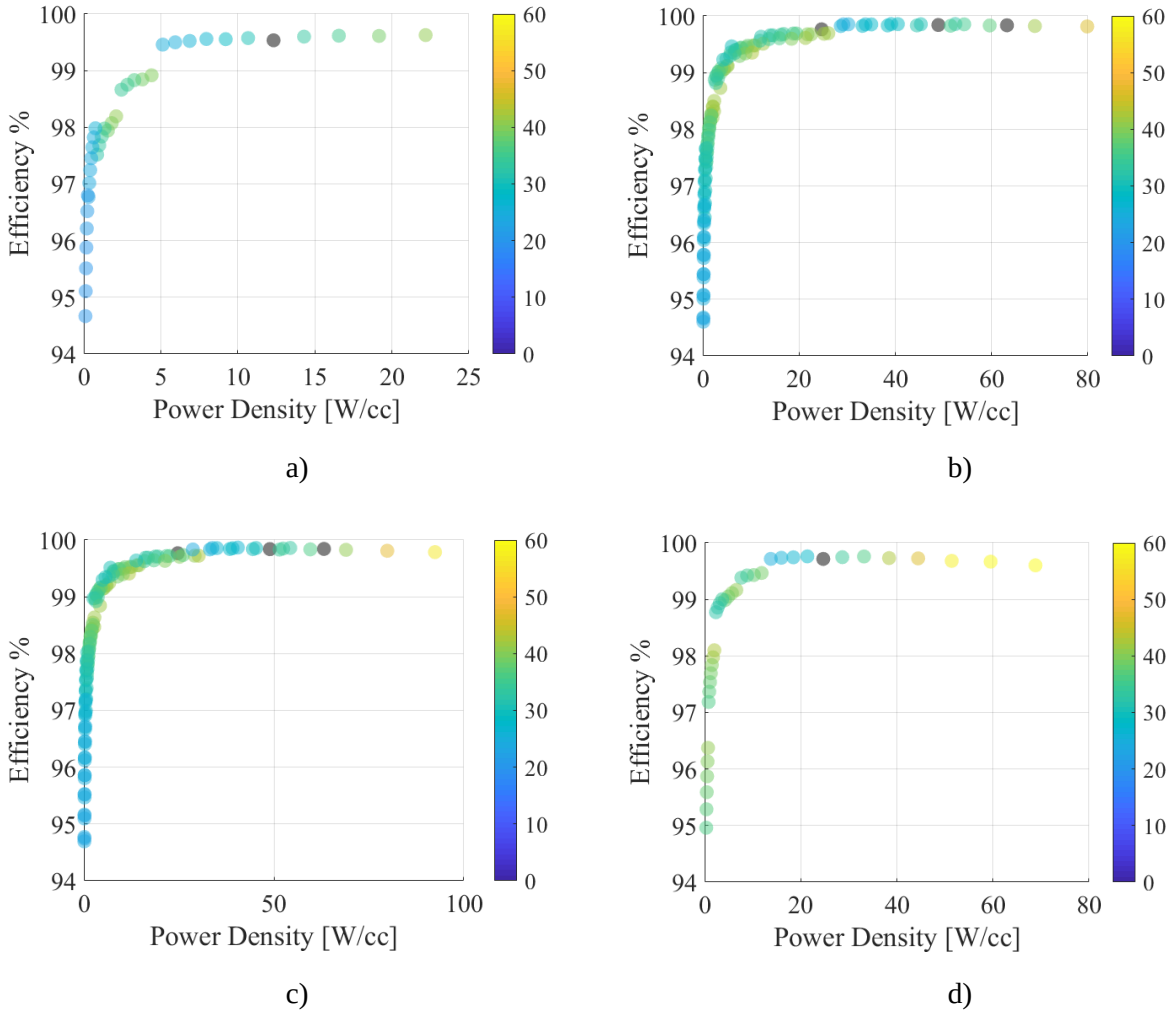

Figure 23: Efficiency-Power density graph for Molypermalloy60 for a) 25kHz, b) 75 kHz, c) 100 kHz and d) 200 kHz

Table 8 clearly shows that increasing the frequency allows designs with higher efficiency and higher power densities. There is, however, a limit to the maximum efficiency. Beyond a certain frequency the efficiency drops, as seen in Table 8 and Figure 23 d). It is also noticeable that more designs are given for 75 kHz than for 25 kHz. This can be explained with equation (35) in 3.2: the largest dimensions a_{ch}, which determine the amount of designs evaluated, are depended on the frequency

Another effect of increasing frequency is a higher temperature rise for higher power densities. Smaller designs for 200 kHz go even beyond 60°C. If a high frequency transformer is needed, the trade-off can be made between high efficiency and lower power density without cooling or lower efficiency and higher power density with a cooling system.

Secondly, for the material Mag-Ferrite F with a relative permeability of 3000 the frequency is also incrementally increased by 25 kHz as can be seen in Table 9. And again, a higher frequency like 200 kHz is added in the last row to show that when the frequency is increased too much, the efficiency goes down.

Table 9: Maximum efficiency and power density for Ferrite F for 25 kHz to 200 kHz

Frequency (kHz)	Max efficiency (%)	Power density (W/cc)
25	99,74	37
50	99,90	52
75	99,91	84
100	99,92	84
200	99,84	33

Based on Table 9 the same conclusions can be made for ferrite F than for the powder iron Molypermalloy 60. Just like before the efficiency and power density increase for higher frequencies, but then drops when the frequency gets too high. The amount of evaluated designs depends on the frequency, as seen in Figure 24.

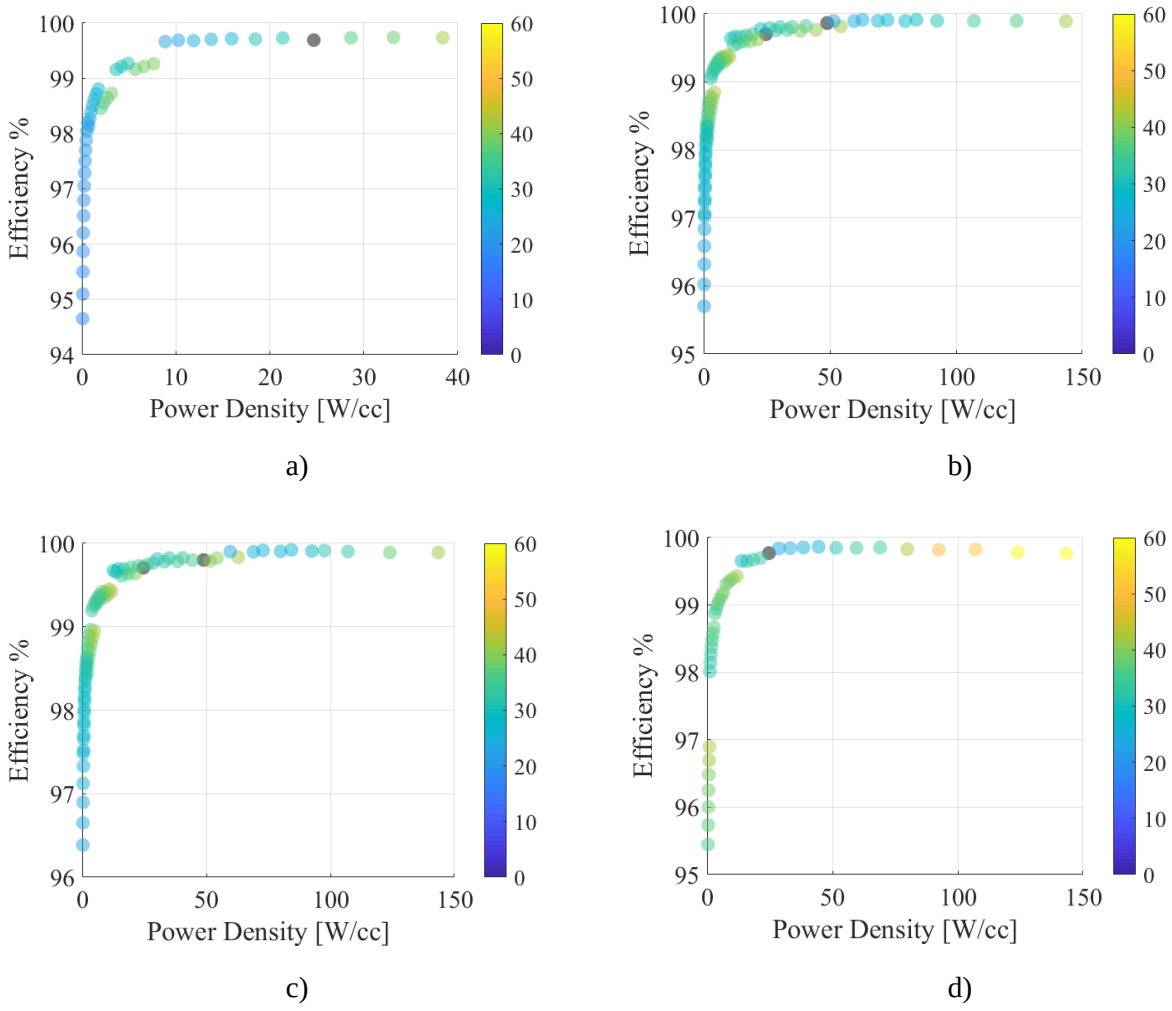

Figure 24: Efficiency-Power density graph for Mag-Ferrite F for a) 25kHz, b) 75 kHz, c) 100 kHz and d) 200 kHz

4.4 Evaluating different designs

So far only graphs for one single material and frequency have been shown. In this section it is made clear that the model can also run through multiple materials and frequencies at once. The results for the entire list of materials from appendix A are shown in Figure 25 for both 100 kHz and 200 kHz. The designs are evaluated for a 10 kW transformer with input voltage of 400 V, output voltage of 800 V and leakage inductance equal to 16 µH.

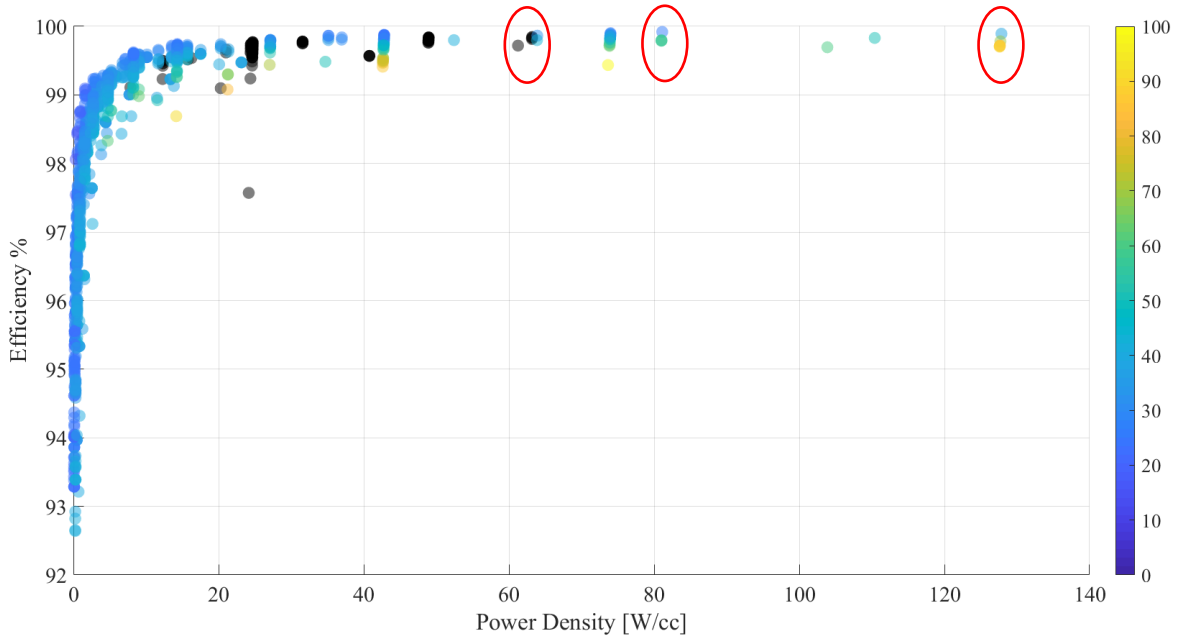

Figure 25: Efficiency-Power density graph for every material for 100 kHz and 200 kHz

A noticeable trend is the drop in efficiency for lower power densities. However, one would expect the opposite to happen; as the core gets bigger, lower losses should occur. An explanation for this could be equation (36), where the total allowed (in the thermally limited approach) or expected (in the non-thermally limited approach) losses are directly proportional to the surface area of the core.

Table 10 shows the parameters for four different designs, which are highlighted on Figure 25. The first design is the one evaluated by the non-thermally limited model with the highest efficiency. It is the blue dot above the green one on the graph. The second and third are the two designs two the far right, with the highest power density. In the final row, the design with the highest efficiency of all thermally limited designs is shown (black dot on the graph).

Table 10: Design comparison for most optimal designs

Core dimensions (mm)	Number of cores	Core material	Frequency (kHz)	Wire diameter	Number of windings (prim/sec)	Efficiency (%)	Power density (W/cc)	Temperature rise (°C)
A=58.75 B=40.00 C=18.33 D=27.67 E=18.25 F=26.67	2	Ferrite F	100	AWG 32	4/8	99.92	81.2	40
A=51.35 B=42.33 C=15.92 D=34.38 E=27.11 F=15.91	2	Ferrite F	100	AWG 32	8/15	99.89	127.99	45
A=51.35 B=42.33 C=15.92 D=34.38 E=27.11 F=15.91	2	Ferrite 3F3	200	AWG 32	7/14	99.70	127.99	85
A=65.00 B=44.20 C=20.00 D=32.80 E=22.20 F=27.40	2	Fair-Rite 77	100	AWG 32	6/11	99.84	63.29	/

The graph shows that at the same power density of 127.99 W/cc, two different materials can be used, both with different efficiencies. It is also useful to see that when someone wants to use Ferrite F at a higher frequency, such as 200 kHz, it is better to use material 3F3 to maintain the same power density. If an external cooling is not desired, the most optimal design in regard to power density and efficiency, is the one shown in the last row in.

The usefulness of having a model that compares different transformer designs can also be seen from this. At the same power density there are different materials with different efficiencies so one can now choose the one with the highest efficiency which results in an efficient use of materials. The use of a cooling system to obtain a higher power density can also be considered here. The temperature rise here also remains relatively low because a low power transformer is used. In a high-power transformer, the temperature rise at high power density will increase more. The non-thermally limited model will be very useful to evaluate these designs with high power density.

As previously mentioned, the dots on the graph represents different materials and core sizes from appendix A. This appendix can be extended with more materials and core sizes to evaluate even more designs. Also, the way the results are presented can be improved in the future to make it more user friendly.

5 Conclusion

As mentioned in chapter 1, the goal of this thesis was to create a tool to optimise the designing process for transformers. In a first step research was done on transformers and how to model them using algorithms. This part is discussed in detail in chapter 2. In this chapter, a modelling flowchart was discussed which would serve as the basis for this thesis's algorithm. It was concluded that Litz wires prove most interesting as these offer the best efficiency. The next chapters therefore focus on using Litz wires for the conductors.

Modelling the transformer was done using two different approaches: thermally limited and non-thermally limited. In the first approach a maximum temperature rise is considered, limiting the amount of cores that can be evaluated. These transformer designs could be useful when no extra cooling system is desired. No temperature limit is assumed in the non-thermally limited approach. This model lets many more designs to be evaluated, though external cooling is required. Chapter 3 explains how both approaches are created using mathematical equations.

The full model is made in Matlab and follows all the steps as discussed in chapter 3. The results are discussed in chapter 4 by comparing graphs for different materials and frequencies. The purpose of this chapter is to show that many different designs can be evaluated and compared and how the tool can be used to choose the most optimal design for a specific application. The results are also validated by creating a flux simulation of the core. Additionally, the results are compared to values from other studies using similar parameters. Another way of validating is building a real transformer and measuring the electrical parameters. However, due to the Covid-19 outbreak this could not be done.

Overall it can be concluded that this master's thesis serves as a good base for future studies on transformer design optimisation. The model created for this thesis gives reliable results. Some future work can improve and optimise the work done in this thesis.

6 Future work

Chapter 4 shows that the transformer model gives reliable results. However, some improvements and changes can be made in the future to improve the model. This thesis only focusses on Litz wires as conductors, though some designs use round, flat or square wires. These different types of wire can be added to the iterative process of the model to study their impact on the losses. Also, only EE-cores are considered. Implementation of other types of cores could also prove interesting as it would give a broader range of options.

In section 2.4.2 the term proximity losses was explained. However, the model does not take this type of copper loss in consideration due to time constraints and the lack of literature of proximity losses in transformer modelling. Other types of losses of which the impact on high power transformers can be evaluated are relaxation and dielectric losses.

For higher power densities, the created algorithm is quite accurate. However, further research and optimisation could be done for lower power densities as the efficiencies here are much lower.

Bibliography

[1] G. Van den Broeck, Voltage Control of Bipolar DC Distribution Systems [Phd Thesis], Arenberg Doctoral School: Faculty of Engineering Science: KU Leuven, 2019.

[2] K. D. Hoang and J. Wang, "Design optimization of high frequency transformer for dual active bridge DC-DC converter," IEEE, Marseille, France, 2012.

[3] Electrical4U, "Magnetic Properties of Engineering Materials," Electrical4U, 3 Novermber 2019. [Online]. Available: https://www.electrical4u.com/magnetic-properties-of-engineering-materials/. [Accessed 9 November 2019].

[4] Encyclopaedia Britannica, "Magnetic permeability," Encyclopaedia Britannica, [Online]. Available: https://www.britannica.com/science/magnetic-permeability. [Accessed 26 October 2019].

[5] C. W. T. McLyman, "Magnetic Materials and Their Characteristics," in *Transfomer and Inductor Design Handbook*, CRC Press, 2016, p. Chapter 2.

[6] G. Vandensande and A. Dexters, Elektriciteit, Diepenbeek: Gezamelijke opleiding Industriële Ingenieurswetenschappen UHasselt & KU Leuven, 1998.

[7] NDT, "The Hysteresis Loop and Magnetic Properties," NDT Resource Center, [Online]. Available: https://www.nde-ed.org/EducationResources/CommunityCollege/MagParticle/Physics/HysteresisLoop.htm. [Accessed 26 October 2019].

[8] Z. P. Soe and Z. W. Thu, "MAKING A SOFT MAGNET (Mn-Zn FERRITE) FOR CORES IN ELECTRONIC COMPONENTS," UNIVERSITY OF TECHNOLOGY (YATANARPON CYBER CITY) FACULTY OF ADVANCED MATERIALS ENGINEERING, 2018.

[9] H. Chan, K. Cheng, T. Cheung and C. Cheung, "Study on Magnetic Materials Used in Power Transformer and Inductor," in *2006 2nd International Conference on Power Electronics Systems and Applications*, Hong Kong, China, IEEE, 2006, pp. 165-169.

[10] B. M. Moskowitz, "Classes of Magnetic Materials," University of Minnesota, [Online]. Available: http://www.irm.umn.edu/hg2m/hg2m_b/hg2m_b.html#diamagnetism. [Accessed 1 November 2019].

[11] Leonardo Energy, "Why use copper rather than aluminium in power transformers?," Leonardo Energy, 14 November 2019. [Online]. Available: https://help.leonardo-energy.org/hc/en-us/articles/206843645-Why-use-copper-rather-than-aluminium-in-power-transformers-. [Accessed 20 November 2019].

[12] A. Williams, "classification of magnetic materials," 2014.

[13] A. Van den Bossche and V. C. Valchev, "Magnetic Core Materials," in *Inductors and transformers for power electronics*, Gent, Taylor & Francis, 2005, pp. 120-134.

[14] K. Daware, "Transformer - Losses And Efficiency," electricaleasy, [Online]. Available: https://www.electricaleasy.com/2014/04/transformer-losses-and-efficiency.html. [Accessed 12 November 2019].

[15] Electrical4U, “Hysteresis Eddy Current Iron or Core Losses and Copper Loss in Transformer,” Electrical4U, 8 June 2019. [Online]. Available: https://www.electrical4u.com/hysteresis-eddy-current-iron-or-core-losses-and-copper-loss-in-transformer/. [Accessed 24 October 2019].

[16] J. Muhlethaler, J. Biela, J. W. Kolar and A. Ecklebe, “Improved Core-Loss Calculation for Magnetic Components Employed in Power Electronic Systems,” *IEEE Transactions on Power Electronics,* vol. 27, no. 2, pp. 964-973, 2011.

[17] R. Ridley, "Proximity Loss in Magnetics Windings," Switching Power Magazine, 2005.

[18] M. Bahmani, Design and Optimization of HF Transformers for High Power DC-DC Applications, Göteborg, Sweden: Chalmers University of Technology, 2014.

[19] M. Bahmani, T. Thiringer and M. Kharezy, “Design Methodology and Optimization of a Medium Frequency Transformer for High Power DC-DC Applications,” *2015 IEEE Applied Power Electronics Conference and Exposition (APEC),* vol. 52, no. 5, pp. 2532-2539, 2015.

[20] E. Iuravin, Transformer Design for Dual Active Bridge Converter, Oxford, Ohio: Miami University, 2018.

[21] A. Van den Bossche and V. C. Valchev, “Fast design approach including eddy current losses,” in *Inductors and transformers for power electronics,* Gent , Taylor & Francis, 2005, pp. 55-119.

[22] Z. Zhang and M. A. E. Andersen, “High Frequency AC Inductor Analysis and Design for Dual Active Bridge (DAB) Converters,” *2016 IEEE Applied Power Electronics Conference and Exposition (APEC),* pp. 1090-1095, 2016.

[23] Ferroxcube, “E100/60/28-3C94,” 2016. [Online]. Available: https://www.digikey.be/product-detail/en/ferroxcube/E100-60-28-3C94/1779-1001-ND/7041461?fbclid=IwAR2QwsNmmD8RywuNxOMwBzqGYgKPU9eTxnimw3tRGmPRkbYNeLV2FCjkOj4. [Accessed 12 March 2020].

[24] A. Van den Bossche and V. C. Valchev, “Thermal Aspects,” in *Inductors and transformers for power electronics,* Gent, Taylor & Francis, 2005, pp. 274-309.

[25] R. J. G. Montoya, High-Frequency Transformer Design for SolidState Transformers in Electric Power Distribution [Thesis], Fayetteville: Master of Science in Electrical Engineering (MSEE): University of Arkansas, 2015.

[26] Pack Litz Wire, “Rupalit Classic,” [Online]. Available: https://www.packlitzwire.com/products/litz-wires/rupalit-classic/. [Accessed 3 March 2020].

[27] Indian Standards Institution, “Pair of E-Cores of Rectangular Section,” in *Guide for calculation of the effective parameters of magnetic piece parts,* New Delhi, Indian Standards Institution, 1977, pp. 10-11.

[28] A. Van den Bossche and V. C. Valchev, “Optimal copper/core loss ratio in magnetic components,” in *Inductors and transformers for power electronics,* Gent, Taylor & Francis, 2005, pp. 386-399.

[29] CSC – IT Center for Science, “Magnetic field induced by harmonic current in a wire,” *Elmer GUI Tutorials,* vol. 1, no. 1, pp. 33-38, 2019.

[30] M. Malinen, J. Ruokolainen and E. Takala, “Computation of Magnetic Fields in 3D,” *Elmer Models Manual,* pp. 110-123, 2020.

[31] V. C. Valchev, T. P. Todorova and A. Van den Bossche, “comparison and design of power electronics transformers in 25kHz-400kHz range,” *2016 19th International Symposium on Electrical Apparatus and Technologies (SIELA),* vol. 1, pp. 354-357, 2016.

[32] C. Nelson, LT1074/LT1076 Design Manual, Milpitas, California, USA: Linear Technology, 1991.

[33] R. Haneda and H. Akagi, “Design and Performance of the 850-V 100-kW 16-kHz Bidirectional Isolated DC-DC Converter Using SiC-MOSFET/SBD H-Bridge Modules,” *IEEE Transactions on Power Electronics,* vol. 35, p. DOI: 10.1109/TPEL.2020.2975256, 2020.

Appendix A: Excel-files

Table A1: Core materials and magnetic properties

Ref	Ref2	K	a	alpha	Beta	Permeability	Loss at 100kHz 500 Gauss (mW/cm3)	Ki	Bmax
Micrometals 8	#8	4,30E-10	8,20E-05	1,13	2,41	35,00	617,00	1,98E-11	0,50
Powdered Iron 18	#18	6,40E-10	1,20E-04	1,18	2,27	55,00	670,00	3,22E-11	0,50
Powdered Iron 26	#26	7,00E-10	1,30E-04	1,36	2,03	75,00	1300,00	4,03E-11	0,50
Powdered Iron 52	#52	9,10E-10	4,90E-04	1,26	2,11	75,00	890,00	5,05E-11	0,50
Magnetics 60	60	2,50E-11	3,20E-06	1,50	2,00	60,00	200,00	1,43E-12	1,05
Kool Mu 75	75	2,50E-11	3,20E-06	1,50	2,00	75,00	200,00	1,43E-12	1,05
Kool Mu 90	90	2,50E-11	3,20E-06	1,50	2,00	90,00	200,00	1,43E-12	1,05
Kool Mu 125	125	2,50E-11	3,20E-06	1,50	2,00	125,00	200,00	1,43E-12	1,05
Molypermalloy 60	–60	7,00E-12	2,90E-05	1,41	2,24	60,00	87,00	3,45E-13	0,80
Molypermalloy 125	–125	1,80E-11	1,60E-04	1,33	2,31	125,00	136,00	8,58E-13	0,80
Molypermalloy 200	–200	3,20E-12	2,80E-05	1,58	2,29	200,00	390,00	1,47E-13	0,80
Molypermalloy 300	–300	3,70E-12	2,10E-05	1,58	2,26	300,00	368,00	1,73E-13	0,80
Molypermalloy 550	–550	4,30E-12	8,50E-05	1,59	2,36	550,00	890,00	1,87E-13	0,80
High Flux 14	–14	1,10E-10	6,50E-03	1,26	2,52	14,00	1330,00	4,59E-12	1,50
High Flux 26	–26	5,40E-11	4,90E-03	1,25	2,55	26,00	740,00	2,21E-12	1,50
High Flux 60	–60	2,60E-11	3,10E-03	1,23	2,56	60,00	290,00	1,06E-12	1,50
High Flux 125	–125	1,10E-11	2,10E-03	1,33	2,59	125,00	460,00	4,32E-13	1,50
High Flux 160	–160	3,70E-12	6,70E-04	1,41	2,56	160,00	1280,00	1,46E-13	1,50
Mag - Ferrite F	F	1,80E-14	1,20E-05	1,62	2,57	3000,00	20,00	3,05E-13	0,50
Mag - Ferrite K	K	2,20E-18	5,90E-06	2,00	3,10	1500,00	5,00	5,20E-20	0,47
Mag - Ferrite P	P	2,90E-17	4,20E-07	2,06	2,70	2500,00	11,00	8,90E-19	0,47
Mag - Ferrite R	R	1,10E-16	4,80E-07	1,98	2,63	2300,00	11,00	3,67E-18	0,47

Philips - Ferrite 3C80	3C80	6,40E-12	7,30E-05	1,30	2,32	2000,00	37,00	3,05E-13	0,45
hilips - Ferrite 3cC8	3C81	6,80E-14	1,50E-05	1,60	2,50	2700,00	38,00	2,68E-15	0,45
Philips - Ferrite 3C85	3C85	2,20E-14	8,70E-08	1,80	2,20	2000,00	18,00	1,02E-15	0,45
Philips - Ferrite 3F3	3F3	1,30E-16	9,80E-08	2,00	2,50	1800,00	7,00	4,66E-18	0,45
TDK - Ferrite PC30	PC30	2,20E-14	1,70E-06	1,70	2,40	2500,00	21,00	9,10E-16	0,25
TDK - Ferrite PC40	PC40	4,50E-14	1,10E-05	1,55	2,50	2300,00	14,00	1,80E-15	0,25
Fair-Rite 77	77	1,70E-12	1,80E-05	1,50	2,30	1500,00	86,00	7,88E-14	0,51
N87	N87	9,49E-10		1,50	2,00	2200,00			0,50

Table A2: Core dimensions for thermally limited model

A(mm)	B	C	D	E	F	Vc(m³)	Ae(m²)
12,70	9,50	3,20	5,70	4,10	6,40	5,59E-07	2,02E-05
14,00	11,00	3,00	3,50	2,00	5,00	2,40E-07	1,45E-05
16,00	11,30	4,70	8,20	5,70	4,70	7,50E-07	2,01E-05
18,00	14,00	4,00	4,00	2,00	10,00	8,00E-07	3,95E-05
19,05	14,33	4,75	8,05	5,69	8,71	1,65E-06	4,13E-05
20,00	14,10	5,90	10,20	7,00	5,90	1,49E-06	3,20E-05
21,80	16,80	5,00	5,70	3,20	15,80	2,04E-06	7,85E-05
25,00	17,50	7,50	12,80	8,70	7,50	2,99E-06	5,20E-05
30,80	19,50	7,20	15,00	9,70	7,30	4,00E-06	6,00E-05
32,00	22,70	9,50	16,40	11,20	9,50	6,18E-06	8,60E-05
36,00	24,50	10,20	21,75	15,75	12,00	1,22E-05	1,26E-04
43,00	29,50	12,20	21,00	14,80	15,20	1,73E-05	1,78E-04
43,00	29,50	12,20	21,00	14,80	20,00	2,27E-05	2,33E-04
43,00	29,50	12,20	32,80	26,00	20,00	3,42E-05	2,36E-04
56,20	37,50	17,20	27,50	18,50	21,00	4,40E-05	3,53E-04
64,00	53,80	10,20	10,20	5,10	50,80	4,07E-05	5,19E-04
65,00	44,20	20,00	32,80	22,20	27,40	7,90E-05	5,40E-04
70,50	48,00	22,00	33,20	21,90	32,00	1,02E-04	6,83E-04
100,30	73,15	27,50	59,40	46,85	27,50	2,02E-04	7,38E-04

Table A 3: Litz wire diameters and number of strands

		Without twists		With twits			
# Individual wires	Single wire nominal diameter	External diameter		External diameter			
				1x52		2x52	
	(mm)	min (mm)	max (mm)	min (mm)	max (mm)	min (mm)	max (mm)
10	AWG 48	0,127	0,142	0,157	0,177	0,187	0,212
20	0,03	0,179	0,2	0,209	0,235	0,239	0,27
25							
30							
35							
45							
60							
75							
90							
105							
120							
135							
180							
225							
270							
10	AWG 46	0,164	0,186	0,194	0,221	0,224	0,256
12	0,04	0,183	0,208	0,213	0,243	0,243	0,278
15		0,201	0,229	0,236	0,269	0,261	0,299
20		0,232	0,264	0,267	0,304	0,292	0,334
25		0,26	0,295	0,295	0,335	0,32	0,365
30		0,284	0,323	0,319	0,363	0,344	0,393
35		0,307	0,349	0,342	0,389	0,367	0,419
45		0,348	0,395	0,383	0,435	0,408	0,465
60		0,405	0,46	0,44	0,5	0,465	0,53
75		0,453	0,515	0,488	0,555	0,513	0,585
90		0,497	0,565	0,532	0,605	0,567	0,645
105		0,537	0,61	0,572	0,65	0,607	0,69
120		0,572	0,65	0,607	0,69	0,642	0,73
135		0,607	0,69	0,642	0,73	0,677	0,77
180		0,722	0,82	0,757	0,86	0,792	0,9
225		0,805	0,915	0,84	0,955	0,895	1,015
270		0,884	1,005	0,919	1,045	0,974	1,105
6	AWG 44	0,162	0,179	0,192	0,214	0,222	0,249
8	0,05	0,186	0,206	0,216	0,241	0,246	0,276
10		0,209	0,231	0,244	0,271	0,269	0,301
12		0,232	0,257	0,267	0,297	0,292	0,327
15		0,256	0,283	0,291	0,323	0,316	0,353
20		0,295	0,327	0,33	0,367	0,355	0,397
25		0,33	0,366	0,365	0,406	0,39	0,436
30		0,382	0,401	0,397	0,441	0,422	0,471
35		0,391	0,433	0,426	0,473	0,451	0,503
45		0,443	0,49	0,478	0,53	0,503	0,56
60		0,515	0,57	0,55	0,61	0,585	0,65
60		0,515	0,57	0,55	0,61	0,585	0,65
75		0,577	0,639	0,612	0,679	0,647	0,719
90		0,633	0,701	0,668	0,741	0,703	0,781

105		0,683	0,756	0,718	0,796	0,753	0,836
120		0,728	0,806	0,763	0,846	0,798	0,886
135		0,773	0,856	0,808	0,896	0,863	0,956
180		0,918	1,017	0,953	1,057	1,008	1,117
225		1,025	1,135	1,06	1,175	1,115	1,235
270		1,126	1,246	1,161	1,286	1,216	1,346
3	AWG 41	0,163	0,189	0,193	0,224	0,223	0,259
5	0,071	0,205	0,238	0,24	0,278	0,265	0,308
6		0,22	0,254	0,255	0,294	0,28	0,324
8		0,253	0,293	0,288	0,333	0,313	0,363
10		0,283	0,328	0,318	0,368	0,343	0,388
12		0,315	0,365	0,35	0,405	0,375	0,435
15		0,347	0,402	0,382	0,442	0,407	0,472
20		0,401	0,464	0,436	0,504	0,461	0,534
25		0,448	0,519	0,483	0,559	0,508	0,589
30		0,491	0,568	0,526	0,608	0,561	0,648
35		0,53	0,614	0,565	0,654	0,6	0,694
45		0,601	0,696	0,636	0,736	0,671	0,776
60		0,699	0,81	0,734	0,85	0,769	0,89
75		0,783	0,906	0,813	0,946	0,873	1,006
90		0,859	0,994	0,894	1,034	0,949	1,094
105		0,927	1,074	0,962	1,114	1,017	1,174
120		0,988	1,144	1,023	1,184	1,078	1,244
135		1,049	1,214	1,084	1,254	1,139	1,314
180		1,246	1,443	1,281	1,483	1,336	1,543
225		1,391	1,61	1,426	1,65	1,481	1,71
270		1,528	1,769	1,563	1,809	1,618	1,869
315		1,649	1,91	1,684	1,95	1,739	2,01
405		1,87	2,165	1,905	2,205	1,96	2,265
420			2,13	- *	- *	- *	- *
525			2,39	- *	- *	- *	- *
630			2,61	- *	- *	- *	- *
735			2,82	- *	- *	- *	- *
840			3,03	- *	- *	- *	- *
945			3,2	- *	- *	- *	- *
1260			3,7	- *	- *	- *	- *
1575			4,15	- *	- *	- *	- *
1890			4,55	- *	- *	- *	- *
2205			4,86	- *	- *	- *	- *
2835			5,6	- *	- *	- *	- *
10	AWG 38	0,407	0,451	0,442	0,491	0,467	0,521
12	0,1	0,452	0,502	0,487	0,542	0,512	0,572
15		0,498	0,553	0,533	0,593	0,568	0,633
20		0,574	0,638	0,609	0,678	0,644	0,718
25		0,642	0,714	0,678	0,754	0,713	0,794
30		0,704	0,782	0,739	0,822	0,774	0,862
35		0,761	0,845	0,796	0,885	0,851	0,945
45		0,862	0,957	0,897	0,997	- *	- *
60		1,003	1,113	1,038	1,153	1,093	1,213
75		1,123	1,246	1,158	1,286	1,213	1,346

90		1,232	1,367	1,267	1,407	1,322	1,467
105		1,33	1,476	1,365	1,516	1,42	1,576
120		1,417	1,573	1,452	1,613	1,507	1,673
135		1,504	1,67	1,539	1,71	1,594	1,77
140			1,65	- *	- *	- *	- *
175			1,83	- *	- *	- *	- *
210			2,01	- *	- *	- *	- *
245			2,16	- *	- *	- *	- *
280			2,34	- *	- *	- *	- *
350			2,62	- *	- *	- *	- *
420			2,95	- *	- *	- *	- *
525			3,27	- *	- *	- *	- *
630			3,59	- *	- *	- *	- *
735			3,87	- *	- *	- *	- *
840			4,19	- *	- *	- *	- *
945			4,4	- *	- *	- *	- *
1050			4,68	- *	- *	- *	- *
1260			5,12	- *	- *	- *	- *
1400			5,49	- *	- *	- *	- *
3	AWG 32		0,49	- *	- *	- *	- *
4	0,2		0,58	- *	- *	- *	- *
5			0,62	- *	- *	- *	- *
6			0,66	- *	- *	- *	- *
7			0,73	- *	- *	- *	- *
8			0,77	- *	- *	- *	- *
9			0,83	- *	- *	- *	- *
10			0,86	- *	- *	- *	- *
15			1,05	- *	- *	- *	- *
20			1,21	- *	- *	- *	- *
25			1,36	- *	- *	- *	- *
30			1,49	- *	- *	- *	- *
35			1,61	- *	- *	- *	- *
40			1,72	- *	- *	- *	- *
45			1,81	- *	- *	- *	- *
50			1,93	- *	- *	- *	- *
60			2,11	- *	- *	- *	- *
80			2,47	- *	- *	- *	- *
90			2,59	- *	- *	- *	- *
100			2,65	- *	- *	- *	- *
105			2,8	- *	- *	- *	- *
120			3	- *	- *	- *	- *
135			3,17	- *	- *	- *	- *
150			3,36	- *	- *	- *	- *
180			3,76	- *	- *	- *	- *
200			3,94	- *	- *	- *	- *
250			4,22	- *	- *	- *	- *
300			4,52	- *	- *	- *	- *
350			4,97	- *	- *	- *	- *
360			5,3	- *	- *	- *	- *
600			7,1	- *	- *	- *	- *

800		7,5	- *	- *	- *	- *
1000		9	- *	- *	- *	- *
1200		10,5	- *	- *	- *	- *
1400		11	- *	- *	- *	- *
3	AWG 27	0,85	- *	- *	- *	- *
4	0,355	1	- *	- *	- *	- *
5		1,07	- *	- *	- *	- *
6		1,14	- *	- *	- *	- *
7		1,26	- *	- *	- *	- *
8		1,32	- *	- *	- *	- *
9		1,42	- *	- *	- *	- *
10		1,47	- *	- *	- *	- *
15		1,81	- *	- *	- *	- *
20		2,08	- *	- *	- *	- *
25		2,33	- *	- *	- *	- *
30		2,56	- *	- *	- *	- *
35		2,76	- *	- *	- *	- *
40		3	- *	- *	- *	- *
45		3,15	- *	- *	- *	- *
50		3,22	- *	- *	- *	- *
60		3,62	- *	- *	- *	- *
75		4,06	- *	- *	- *	- *
	AWG 26 0,452 AWG 25 0,505 AWG 24 0,566 AWG 23 0,632 AWG 22 0,701 AWG 21 0,785 AWG 20 0,874 AWG 19 0,948 AWG 18 1,09					

AWG 17 1,22 AWG 16 1,37 AWG 15 1,53 AWG 14 1,71 AWG 13 1,9

Appendix B: Simulation parameters

Table B 1: Simulation bodies

	Body 1	**Body 2**	**Body 3**	**Body 4**
Assignment	Primary winding	Core	Secondary winding	Surrounding air
material	Copper	Molypermalloy 300	Copper	/
Solver 1	MagnetoDynamics	MagnetoDynamics	MagnetoDynamics	MagnetoDynamics
Solver 2	ResultOutputSolve	ResultOutputSolve	ResultOutputSolve	ResultOutputSolve
Solver 3	MagnetoDynamics-CalcFields	MagnetoDynamics-CalcFields	MagnetoDynamics-CalcFields	MagnetoDynamics-CalcFields
Boundary conditions	Boundary condition 1	/	Boundary condition 2	Boundary condition 3

```
Simulation
  Max Output Level = 5
  Coordinate System = Cartesian
  Coordinate Mapping(3) = 1 2 3
  Simulation Type = Steady state
  Steady State Max Iterations = 1
  Output Intervals = 1
  Timestepping Method = BDF
  BDF Order = 1
  Coordinate Scaling = 1.0e-3
  Angular Frequency = 125663
  Solver Input File = case.sif
  Post File = case.vtu
```

```
Solver 1
  Equation = MgHarm
  Procedure = "MagnetoDynamics"
"WhitneyAVHarmonicSolver"
  Exec Solver = Always
  Stabilize = True
  Bubbles = False
  Lumped Mass Matrix = False
  Optimize Bandwidth = True
  Steady State Convergence Tolerance = 1.0e-5
  Nonlinear System Convergence Tolerance = 1.0e-7
  Nonlinear System Max Iterations = 20
  Nonlinear System Newton After Iterations = 3
  Nonlinear System Newton After Tolerance = 1.0e-3
  Nonlinear System Relaxation Factor = 1
  Linear System Solver = Iterative
  Linear System Iterative Method = BiCGStabl
  Linear System Max Iterations = 500
  Linear System Convergence Tolerance = 1.0e-10
  BiCGstabl polynomial degree = 4
  Linear System Preconditioning = none
  Linear System ILUT Tolerance = 1.0e-3
  Linear System Abort Not Converged = False
  Linear System Residual Output = 10
  Linear System Precondition Recompute = 1
```

```
Solver 2
  Equation = Result Output
  Output Format = Vtu
  Output File Name = case
  Discontinuous Bodies = True
  Procedure = "ResultOutputSolve"
"ResultOutputSolver"
  Exec Solver = After Simulation
```

```
Solver 3
  Equation = MgDynPost
  Calculate Current Density = True
  Procedure = "MagnetoDynamics"
"MagnetoDynamicsCalcFields"
  Calculate Magnetic Field Strength = True
  Discontinuous Bodies = True
  Exec Solver = Before Saving
  Stabilize = True
  Bubbles = False
  Lumped Mass Matrix = False
  Optimize Bandwidth = True
  Steady State Convergence Tolerance = 1.0e-5
  Nonlinear System Convergence Tolerance = 1.0e-7
  Nonlinear System Max Iterations = 20
  Nonlinear System Newton After Iterations = 3
```

```
  Nonlinear System Newton After Tolerance = 1.0e-3
  Nonlinear System Relaxation Factor = 1
  Linear System Solver = Iterative
  Linear System Iterative Method = BiCGStab
  Linear System Max Iterations = 500
  Linear System Convergence Tolerance = 1.0e-10
  BiCGstabl polynomial degree = 2
  Linear System Preconditioning = ILU0
  Linear System ILUT Tolerance = 1.0e-3
  Linear System Abort Not Converged = False
  Linear System Residual Output = 10
  Linear System Precondition Recompute = 1

Boundary Condition 1
  Target Boundaries(1) = 7
  Name = "Current_primary"
  Electric Current Density = 11800000

Boundary Condition 2
  Target Boundaries(1) = 6
  Name = "Current_secundary"
  Electric Current Density = 16e6

Boundary Condition 3
  Target Boundaries(7) = 1 5 12 32 35 36 40
  Name = "Farfield"
  AV re {e} 2 = 0
  AV im {e} 1 = 0
  AV re {e} 1 = 0
  AV im {e} 2 = 0
```